DEUTSCHES ELEKTRONEN-SYNCHROTRON DESY

DESY 74/5
February 1974

Electroproduction in a Streamer Chamber: Multiplicities, Inclusive Cross Sections and Production of ρ^0 and ω Mesons

by

V. Eckardt, H. J. Gebauer, P. Joos, A. Ladage, H. Meyer, B. Naroska
D. Notz, W. J. Podolsky, P. Stein, G. Wolf, and S. Yellin
Deutsches Elektronen-Synchrotron DESY, Hamburg

G. Drews, J. Knobloch, H. Nagel, E. Rabe, C. Sander, H. Spitzer, and K. Wacker
II. Institut für Experimentalphysik der Universität Hamburg

2 HAMBURG 52 · NOTKESTIEG 1

DESY 74/5
February 1974

Electroproduction in a Streamer Chamber: Multiplicities, Inclusive Cross Sections and Production of ρ^0 and ω Mesons

by

V. Eckardt, H. J. Gebauer, P. Joos, A. Ladage, H. Meyer, B. Naroska
D. Notz, W. J. Podolsky, P. Stein, G. Wolf, and S. Yellin
Deutsches Elektronen-Synchrotron DESY, Hamburg

G. Drews, J. Knobloch, H. Nagel, E. Rabe, C. Sander, H. Spitzer, and K. Wacker
II. Institut für Experimentalphysik der Universität Hamburg

Electroproduction in a Streamer Chamber: Multiplicities, Inclusive Cross Sections and Production of ρ^o and ω Mesons

V. Eckardt*, H.J. Gebauer*, P. Joos, A. Ladage, H. Meyer**, B. Naroska***, D. Notz, W.J. Podolsky+, P. Stein++, G. Wolf, and S. Yellin
Deutsches Elektronen-Synchrotron DESY, Hamburg, Germany

G. Drews, J. Knobloch, H. Nagel, E. Rabe, C. Sander, H. Spitzer, and K. Wacker
II. Institut für Experimentalphysik der Universität Hamburg, Hamburg, Germany

Abstract:

Hadron production by ep scattering in the kinematical region $0.3 < Q^2 < 1.5$ GeV^2 and $1.3 < W < 2.8$ GeV was studied with a streamer chamber at DESY. The average multiplicity of charged hadrons, $\langle n \rangle$, is consistent with a logarithmic s dependence: $\langle n \rangle = (0.79 \pm 0.11) + (0.93 \pm 0.06) \ln(\omega'-1) + (1.04 \pm 0.08) \ln Q^2/m_p^2 \approx 0.8 + \ln s/m_p^2$. The multiplicity does not scale with respect to ω' or ω_W. Inclusive π^- production was analyzed in terms of $(x,p_\perp^2)$ and (M_X,t) as a function of Q^2,W and Q^2,ω'. In the central and the target fragmentation region no Q^2 dependence was found. The reduction of the π^- yield in the beam fragmentation region compared to photoproduction can be related to the smaller ρ^o cross section in electroproduction. The normalized invariant π^- cross section, F(x), does not scale with respect to ω' in our kinematical range. In the non diffractive region, $2.5 < \omega' < 10$, the slope of the $p_\perp^2$ distribution decreases with Q^2 for fixed ω'. In the diffractive region, $10 < \omega' < 15$, the effect is small. In the beam fragmentation region a longitudinal/transverse interference term was observed. The Q^2 dependence of $\sigma(\gamma_V p \to \rho^o p)$ for $W > 2$ GeV is essentially determined by the ρ propagator as suggested by VDM. The slope of $d\sigma/dt$, for ρ^o production at $\langle Q^2 \rangle = 0.4$ GeV^2 is smaller than at $Q^2 = 0$. For $W > 2.2$ GeV the ρ^o polar decay angular distribution shows a nonzero longitudinal part, $r_{oo}^{04} = 0.183 \pm 0.031$, while the distribution of the angle ψ, sensitive to linear photon polarisation, implies dominant production by transverse photons.

---

* Now at Max-Planck-Institut für Physik und Astrophysik, München
** Now at UC Santa Cruz, CA, USA
*** Now at CERN, Geneva
\+ Now at University of Washington, Seattle, Washington, USA
\+\+ On leave of absence from Cornell University, Ithaca, NY, USA

The s- channel helicity flip amplitudes are small compared to non flip amplitudes. Assuming SCHC we find for ρ^o production $R = \sigma_L/\sigma_T = 0.260 \pm 0.054$ for $\langle W \rangle = 2.45$ and $\langle Q^2 \rangle = 0.5$ GeV^2. Interference between production by longitudinal and transverse photons was found. Assuming SCHC and only natural parity exchange the phase between the two amplitudes was found to be $\cos\delta = 0.61 \pm 0.15$. A pronounced ω peak was seen in the reaction $\gamma_V p \to p\pi^+\pi^-\pi^o$. The Q^2 and W dependence of $\sigma(\gamma_V p \to \omega p)$ was determined.

Introduction

In this paper we report on the gross features of electroproduced final states such as the behaviour of multiplcities, the topological cross sections and the inclusive π^- momentum spectra, and on rho and omega production[1].

The data come from the DESY streamer chamber experiment designed to detect all charged hadrons produced in an ep collision. Details of the experiment and first results have been given elsewhere.[2] A 7.2 GeV electron beam is passed through a 9 cm long liquid hydrogen target located inside a 1 m long streamer chamber situated in a 18 kG magnet. A scintillator-shower counter hodoscope detects the scattered electron and triggers the chamber. The analysis of the photographs is similar to the evaluation of bubble chamber film. Approximately 400 000 pictures have been taken corresponding to a total flux of $4 \cdot 10^{12}$ electrons.

The present results are obtained from an analysis of 15 600 measured events corresponding to 25 % of the total number of available events. After the appropriate cuts for pulse heights, acceptance etc. were made, 6500 inelastic events remained in the Q^2,W region (W is the cms energy of the hadron system) 0.3 - 1.5 GeV^2, 1.3 - 2.8 GeV. For the determination of cross sections, multiplcities and inclusive spectra only 55 % of these events were used.

In the distributions shown below each event was weighted by the proper acceptance and by a factor taking into account radiative corrections. Events from elastic ep scattering were removed by means of a coplanarity cut. For details see Ref. 2.

1. Total Cross Sections

We determined the sum of the total transverse and longitudinal cross sections, $\sigma_T + \varepsilon\sigma_L$ (as defined by Hand[3]) for virtual photon proton scattering and compared our values to those of previous experiments. This serves as a check on our data taking and analysis procedure. Fig. 1 shows good agreement between the different experiments.[4-6]

2. Hadron Multiplicity and Topological Cross Sections

We analyzed the charged hadron multiplcity $\langle n \rangle$,

$$\langle n \rangle = \frac{\sum n \cdot \sigma_n}{\sigma_{tot}} \qquad (1)$$

where σ_n is the cross section for producing n charged hadrons, as a function of Q^2, s and the scaling variables ω' and ω_W.

$$s = W^2$$

$$\omega' = W^2/Q^2 + 1$$

$$\omega_W = \frac{(W^2 - m_p^2 + Q^2) + m_W^2}{Q^2 + a^2} \quad \text{with } m_W^2 = 1.43 \text{ GeV}^2 \text{ and } a^2 = 0.42 \text{ GeV}^2.\ ^{7}$$

We considered both scaling variables since they behave qualitatively different in the small Q^2 region. The variable ω_W connects electroproduction with photoproduction while ω' does not. The use of ω_W is suggested by the generalized vector dominance model[8,9]. In Table I we give the mean values of Q^2,W,ω',ω_W for different kinematical regions we use below.

a) $\langle n \rangle$ as a function of W and Q^2

In Fig. 2a the mean charged multiplicity $\langle n \rangle$ is plotted for fixed W as a function of Q^2 together with photoproduction data.[12] At higher energies ($W \geq 1.8$ GeV) the electroproduction values for $Q^2 < 1$ GeV^2 are lower by approximately 10 % than those for $Q^2 = 0$. This behaviour becomes somewhat clearer when we look at the Q^2 dependence of the normalized topological cross sections, σ_n/σ_{tot}, shown in Fig. 3 (the curves are drawn to guide the eye): the decrease

in <n> is caused by an increase in the production of reactions with one charged hadron in the final state (one-prong events) and a drop in the 3-prong cross section. Beyond $Q^2 = 0.6$ GeV^2 the Q^2 variation is reversed: $\sigma_{1prong}/\sigma_{tot}$ decreases while $\sigma_{3prong}/\sigma_{tot}$ increases. The 5-prong rate does not show a significant Q^2 dependence.

A qualitative explanation for this behaviour may be found in two phenomena: with increasing Q^2 less ρ^o and ω-mesons are being produced in $\gamma_V p \to \rho^o(\omega) p$ [2] (see below) causing a reduction of σ_3/σ_{tot}. The 1-prong cross section receives a large contribution from longitudinal photons. This has been observed for single pion electroproduction[13] ($\gamma_V p \to \pi^+ n$) and may be true also for other one-prong reactions.

In Fig. 2b <n> is shown for fixed Q^2 as a function of $s = W^2$ together with data from SLAC.[10] In the kinematical region $s < 20$ GeV^2, $Q^2 < 1.5$ GeV^2 the charged multiplicity follows a simple ln s law. We will return to this point later.

b) <n> as a function of ω' and Q^2

In Fig. 4a,b the charged multiplicity for fixed ω' intervals is plotted as a function of Q^2 and for fixed Q^2 intervals as a function of ω'. Note that in the lowest ω' interval the central ω' value changes somewhat with Q^2 (see also Table I). We conclude from Fig. 4 that the data are consistent with $\langle n \rangle \sim \ln Q^2$ for ω' fixed.

Our data may be compared with various theoretical predictions which were made for the deep inelastic region:

$\langle n \rangle \sim$ constant + ln ω'	Drell-Levy-Yan[14]
$\langle n \rangle \sim s^{\alpha(\omega')}$	Chou-Yang[15]
$\langle n \rangle \sim \ln(\omega'-1) + \ln Q^2$	Bjorken[16]

Our data favor the last model. In photoproduction the average charge multiplicity was found to behave like[11]

$$\langle n \rangle = C_o + C_s \ln s/m_p^2 \text{ with } C_o \approx 1,\ C_s \approx 1 \qquad (2)$$

which in terms of electroproduction variables reads

$$\langle n \rangle = C_o + C_s \ln \frac{(\omega' - 1)\, Q^2}{m_p^2} \qquad (3)$$

m_p = mass of the proton

Using Eq(3) as a guide the following expression was fitted to our data:

$$\langle n \rangle = C_o + C_\omega \ln (\omega' - 1) + C_Q \ln Q^2/m_p^2 \qquad (4)$$

From a fit to the data shown in Fig. 4 the following values for the parameters were obtained:

$$C_o = 0.79 \pm 0.11 , \quad C_\omega = 0.93 \pm 0.06 , \quad C_Q = 1.04 \pm 0.08.$$

We see that the behaviour of the charged multiplicity can be described by the simple expression Eq(2) to within 10 %, and that for s fixed no strong Q^2 dependence is observed. Preliminary data from a Cornell experiment show a similar trend at larger values of Q^2.[17]

Finally, in Fig. 5 we look at the Q^2 behaviour of the topological cross sections for fixed ω' intervals (ω': 2.5 - 6, 6 - 10, 10 - 15); in all three intervals $\sigma_{1prong}/\sigma_{tot}$ shows the same logarithmic decrease with Q^2, while $\sigma_{3prong}/\sigma_{tot}$ in the kinematical region studied does not exhibit a simple pattern.

c) <n> as a function of ω_W and Q^2

In Fig. 6 we studied the charged multiplicity as a function of Q^2 and the scaling variable ω_W. It is evident that the charged multiplicity does not scale with ω_W (although νW_2 does scale with respect to ω_W in this kinematical region[7]). Qualitatively, <n> behaves like

$$\langle n \rangle \sim \text{const} + \text{const} \cdot Q^2 \qquad \text{for fixed } \omega_W$$

$$\langle n \rangle \sim \text{const} + \text{const} \cdot \ln \omega_W \qquad \text{for fixed } Q^2$$

3. Inclusive π^- production, $\gamma_V p \to \pi^- X$

The π^- momentum spectra were described in terms of the following two sets of variables: $(x, p_\perp^2)$ and (M_X, t).

$x = p_{\parallel}^*/p_{max}^*$

$p_{\parallel}^*$ = longitudinal momentum of π^-

p_{max}^* = maximum possible momentum of π^- } in the hadron cms

$y_{lab} = \frac{1}{2} \ln \frac{E + p_{\parallel}}{E - p_{\parallel}}$, where $E, p_{\parallel}$ are the π^- energy and longitudinal momentum in the lab system

$p_\perp$ = π^- transverse momentum

M_X = effective mass of the system X recoiling against the π^-

t = square of the four momentum transfer between virtual photon and π^-.

Expressed in terms of the four momenta of γ_V, target proton p and π^-:

$M_X^2 = (\gamma_V + p - \pi^-)^2$, $t = (\gamma_V - \pi^-)^2$.

Depending on which picture is being tested one set of variables is favored over the other: For example the Q^2 dependence of the target and beam fragmentation region and of the central region is studied best with respect to x or y, while for comparison with Regge models the variables M_X and t appear to be better suited. The π^- distributions were determined on the assumption that all negative hadron tracks belong to negative pions. From the observed K^- decays we can place an upper limit of 8 % on the K^- contamination.

a) π^- production as a function of W and Q^2

The invariant normalized cross section, defined as

$$F(x) = \frac{1}{\sigma_{tot}} \frac{1}{\pi} \int_0^{p_{\perp max}^2} \frac{E^*}{p_{max}^*} \frac{d\sigma}{dx dp_\perp^2} dp_\perp^2 \qquad (5)$$

$E^* = \pi^-$ cms energy

is shown in Fig. 7 for different W intervals (1.5 - 1.8 GeV, 1.8 - 2.2 GeV and 2.2 - 2.8 GeV) and for two different Q^2 intervals (0.3 - 0.5 GeV^2 and

0.5 - 1.5 GeV^2). For the highest W bin also photoproduction data[12] are shown. The conclusions are similar to those in our previous publication[2]: Within the present statistical accuracy no significant differences between the $\langle Q^2 \rangle$ = 0.4 and 0.8 GeV^2 spectra exist. Comparison with photoproduction at $\langle W \rangle$ = 2.48 GeV shows that in the target fragmentation ($x \lesssim -0.3$) and central region ($-0.2 \lesssim x \lesssim 0.2$) F(x) is the same for photo- and electroproduction. In the beam fragmentation ($x \gtrsim 0.3$) the π^- yield drops by a factor of 1.5 - 2.0 going from photo- to electroproduction.

Most of this effect is due to the reduction in the ρ^o contribution to σ_{tot} with increasing Q^2 (see below) as demonstrated by Fig. 7d where the ρ^o contribution ($\gamma_V p \to \rho^o p$) has been removed from both the photo- and electroproduction points.

Next we turn to the Q^2 dependence of the transverse momentum distribution. Fig. 8 displays $p_\perp^2$ distributions for the central and beam fragmentation regions for various Q^2,W intervals. Also indicated are the exponential slopes obtained from fits of the form C exp($Ap_\perp^2$) (see Table II). For fixed W, within the present errors, the slope A is found to be the same for $\langle Q^2 \rangle$ = 0.4 and 0.8 GeV^2 in both x regions. However, when the hadron cms energy W decreases from 2.45 to 1.65 GeV, in the central region A increases from ~8 - 9 GeV^{-2} to ~14 GeV^{-2}. Most probably this is a phase space effect: at low energies the W value is too small to allow larger values of $p_\perp^2$.

For completeness, we give in Fig. 9 the rapidity distributions for different Q^2 regions.

b) π^- production as a function of ω' and Q^2

In order to test for scaling the π^- spectra were analyzed also as a function of ω' and Q^2. The data were grouped into three ω' intervals: ω' = 2.5 - 6 (non diffractive region), ω' = 6 - 10 (transition region from the non diffractive to the diffractive region) and ω' = 10 - 15 (diffractive region). For the following discussion it is useful to keep in mind that for fixed ω' the hadron cms energy (W) increases with Q^2 (see e.g. Table I).

Fig. 10 shows the invariant normalized cross section F(x) for different ω' and Q^2 bins. F(x) is found to grow with Q^2 in the central region, i.e. F(x) does not scale in the Q^2 region under study. The hump in F(x) near $x \approx 0.7$, most noticeably for $6 < \omega' < 10$, is due to Δ^{++} production ($\gamma_V p \to \pi^- \Delta^{++}$).

A dramatic change with Q^2 is seen in the $p_\perp^2$ distributions for the central region (Fig. 11): they become broader with increasing Q^2. The exponential slope A for $\omega' < 10$ changes by roughly a factor of two from $A \approx 15$ GeV^{-2} to $A \approx 7 - 8$ GeV^{-2} between $\langle Q^2 \rangle \sim 0.5$ and 1 GeV^2. Table III contains the forward cross sections and slopes obtained by exponential fits. Since the forward cross sections stays constant we conclude that for ω' fixed with increasing Q^2 additional π^-'s with larger $p_\perp^2$ values are being produced which cause the observed widening of the $p_\perp^2$ distribution. Most likely this drastic variation has to be attributed to phase space, since for fixed ω', the hadron cms energy W increases with Q^2.

In the so called diffractive region ($10 < \omega' < 15$) the change in slope is small (Fig. 11).

In certain parton models[16,18] the average transverse momentum of forward produced particles at fixed ω' is predicted to increase proportionally with the longitudinal cms momentum. Fig. 12 shows $\langle p_\perp \rangle$ and $\langle p_\parallel^* \rangle$ ($x > 0$, no limit in $p_\perp$) as a function of Q^2 for different ω' intervals: $\langle p_\perp \rangle$ is indeed rising with Q^2 like the average longitudinal momentum.

c) $\bar{\pi}$ production as a function of M_X and t

In Fig. 13 we present the missing mass spectrum recoiling against the π^-. The normalized cross section $\frac{1}{\pi\sigma_{tot}} \frac{d\sigma}{dM_X}$ has been plotted for fixed W,Q^2 (Fig. 13) and fixed ω',Q^2 (Fig. 14) intervals. It is remarkable that for fixed W the mass spectrum does not change with Q^2 except for a possible 10 - 20 % decrease with increasing Q^2 near the high mass end. For a given ω' interval the mass spectrum is displaced towards higher masses when Q^2 increases, which is a reflection of the increasing cms energy.

Fig. 15 shows a Chew-Low plot of the four momentum transfer t versus missing mass M_X. Due to the phase space limitations the minimum value of $|t|$ increases drastically with larger values of M_X. Fig. 16 shows the projections onto the t axis for certain M_X intervals.

d) Φ dependence of π^- production

In the present experiment both, transverse and longitudinal photons can contribute to hadron production; the ratio of the longitudinal to transverse photon flux is $\varepsilon = 0.9$ averaged over the Q^2,W region accepted. Production by transverse photons can lead to an anisotropic distribution of the π^- production plane relative to the electron scattering plane. If Φ is defined to be the angle between the two planes, $\cos\Phi = \dfrac{(e \times e')\cdot(\gamma_V \times \pi^-)}{|e \times e'|\cdot|\gamma_V \times \pi^-|}$, the Φ distribution has the general form

$$W(\Phi) = 1 + C_p\, \varepsilon\cos 2\Phi + \sqrt{2\varepsilon(\varepsilon+1)}\, C_I \cos\Phi \,. \qquad (6)$$

Longitudinal photons contribute to the constant term, transverse photons to the constant term and to C_p, and C_I arises from longitudinal/transverse interference.

In Fig. 17 we look at the distribution of the angle Φ versus x for all π^- from $1.8 < W < 2.8$ GeV and $0.3 < Q^2 < 1.5$ GeV^2. While the target fragmentation and central regions show a roughly constant Φ distribution, the π^- for $x > 0.4$ are emitted more frecuently under $\Phi > 90^\circ$. Figs. 18a,b show Φ vs W for the central and the beam fragmentation region. Above $W = 1.8$ GeV the Φ distribution appears to be independent of W. For $0.3 < x < 0.7$ a preference for Φ values close to 180° is seen. Fig. 19 shows $W(\Phi)$ for the central region in two regions of Q^2.

In Fig. 20a $W(\Phi)$ is given for the beam fragmentation region together with a fit of Eq(6) to the data. The fit yielded

$$C_p = 0.40 \pm 0.09$$
$$C_I = -0.23 \pm 0.05$$

establishing the presence of an interference between production by longitudinal and transverse photons. We investigated to what extent the observed Φ anisotropy has its origin in ρ^o production ($\gamma_V p \to \rho^o p$) which has been found to emit the decay pions preferentially in the electron scattering plane ($\Phi = 0^\circ$, 180°) and which shows longitudinal/transverse interference[2] (see below). Fig. 20b shows the π^- distribution without ρ^o events, and for ρ^o events alone. We conclude that the observed Φ anisotropy is not contributed by ρ^o events alone.

Craigie, Kramer and Körner[19], on the basis of a Regge pole model, have argued that close to x = 1, π^- production by longitudinal photons should be dominant. On the other hand, in the central region where most of the cross section is found, transverse photons must dominate since for the total cross section $\sigma_L << \sigma_T$. Our data support this picture in the sense that in between the central region and x = 1 we find both transverse and longitudinal contributions to be present.

4. Rho production

We analyzed ρ^o meson production via

$$\gamma_V p \to \rho^o p \tag{7}$$

in the final state

$$ep \to ep\pi^+\pi^-. \tag{8}$$

The analysis procedure has been described in Ref. 2. In the kinematical region: $1.3 < W < 2.8$ GeV, $0.3 < Q^2 < 1.5$ GeV^2 2100 events were obtained which fitted reaction (8) and for which the track ionisation observed agreed with that predicted by the fit. In order to check the fit procedure and to determine the corrections for radiative effects for measuring errors and for multiple scattering of the outgoing particles for reaction (7), events were generated with the program STYX[20] which simulates our setup. The correction factor which previously has been estimated[2] to be 16 ± 5 % turned out to be 16, 15 and 5 % for the W intervals 1.7 - 2, 2.0 - 2.2 and 2.2 - 2.8 GeV, respectively.

a) Mass Distributions

In Figs. 21 and 22 the mass spectra of the $p\pi^+$, $p\pi^-$ and $\pi^+\pi^-$ systems are displayed for the higher W intervals and for different Q^2 regions. Close to the ρ threshold (W ≃ 1.7 GeV) strong Δ^{++} and ρ^o production is observed. At energies above W = 2 GeV the rho contribution dominates while Δ^{++} production becomes less important. A cut on forward produced ($\pi^+\pi^-$) pairs reduces the background underneath the rho to a small level (see shaded histograms).

b) Cross Sections

The cross sections for Δ^{++}, Δ^{o} and ρ^{o} production were determined[21] by a maximum-likelihood fit to the Dalitz plot density $dN(M^2_{p\pi^+}, M^2_{\pi^+\pi^-})$:

$$dN(M^2_{p\pi^+}, M^2_{\pi^+\pi^-}) = \Big[a_{\Delta^{++}} f_{\Delta^{++}}(M_{p\pi^+}) + a_{\Delta^o} f_{\Delta^o}(M_{p\pi^-}) + a_\rho f_\rho (M_{\pi^+\pi^-}) W(\cos\Theta_H) + a_{ps} f_{ps} \Big] dM^2_{p\pi^+} dM^2_{\pi^+\pi^-} \quad (9)$$

The a's are fit parameters and measure the size of the individual contributions; $f_{\Delta^{++}}$, f_{Δ^o} and f_ρ represent the corresponding Breit-Wigner terms; the ρ-Breit-Wigner was multiplied by a factor $(M_\rho / M_{\pi^+\pi^-})^4$. The polar decay angular distribution, $W(\cos\Theta_H)$, for ρ^o events in the helicity system was included in the fit since $W(\cos\Theta_H)$ is strongly affected by contributions from Δ^{++} and Δ^o production. The expression for $W(\cos\Theta_H)$ in terms of the ρ density matrix element r^{o4}_{oo} (see Ref. 22) is:

$$W(\cos\Theta_H) = 3/4 \cdot \{1 - r^{o4}_{oo} + (3r^{o4}_{oo} - 1)\cos^2\Theta_H\} \quad (10)$$

In order to determine r^{o4}_{oo} for a given W interval all events between $0.3 < Q^2 < 1.5$ GeV^2 were used. Then the events in the three Q^2 intervals 0.3 - 0.5 GeV^2, 0.5 - 0.8 GeV^2 and 0.8 - 1.5 GeV^2 were fitted separately with r^{o4}_{oo} fixed to the value obtained in the previous fit. The results are given in Table IV and shown by the curves in Figs, 21, 22 and 25 (see below). The fitted curves describe the mass distributions well.

Fig. 23 displays the ρ^o cross section for different W intervals as a function of Q^2. Ahrens et al.[23] have measured the sum of the ρ^o and ω cross sections. In order to deduce from these data the ρ^o cross sections we used our data on ω production (see below) and subtracted the ω contribution. The resulting ρ^o cross sections agree with ours (see Fig. 23). The ρ^o cross section is seen to decrease rapidly with Q^2, e.g. at $W \approx 2.5$ GeV by a factor of ten between $Q^2 = 0$ and 1 GeV^2. This sharp drop reflects itself also in the Q^2 dependence of the ratio of the ρ^o cross section to the total cross section (see Table V). For $\langle W \rangle = 2.45$ GeV and Q^2 between 0 and 1 GeV^2 the ρ^o fraction changes from 16.0 ± 0.8 % to 1.9 ± 1.1 %.

The VDM prediction for the Q^2 dependence of σ_ρ is shown by the curves in Fig,23. They were calculated from the following expression[24]:

$$\sigma_{\gamma_V p \to \rho^o p}(Q^2,W) = \frac{p^*_{in}(Q^2 = 0)}{p^*_{in}(Q^2)} \left(\frac{m_\rho^2}{m_\rho^2 + Q^2}\right)^2 \left\{1 + \varepsilon \xi^2 \frac{Q^2}{m_\rho^2}\right\} *$$

$$* \sigma_{\gamma p \to \rho^o p}(Q^2 = 0,W) \exp(At_{min}) \qquad (11)$$

where p^*_{in} is the photon momentum in the hadron cms, $p^*_{in}(Q^2 = 0)/p^*_{in}(Q^2) = (W^2 - m_p^2)/\{(W^2 - m_p^2 - Q^2)^2 + 4W^2Q^2\}^{1/2}$.

The ratio of p^*_{in} enters Eq(11) because of the difference in photon flux for different Q^2 at a given value of W. The parameter ξ^2 measures the relative size of elastic longitudinal and transverse vectormeson nucleon scattering. We put $\xi^2 = R\ m_\rho^2/\langle Q^2\rangle \approx R$ where R is the ratio of the ρ production cross sections for longitudinal and transverse photons; R was taken from the analysis of the decay angular distribution assuming s-channel helicity conservation (SCHC) in ρ^o production (see below). The factor $\exp(At_{min})$ corrects for the $|t|_{min}$ cutoff. The VDM expression Eq(11), in essence the ρ^o propagator, is seen to account rather well for the large reduction in ρ^o production with increasing Q^2 (see Fig. 23). On the other hand, our data are also compatible with the following functional form proposed by Preparata[26]:

$$\frac{d\sigma}{dt}(\gamma_V p \to \rho p) = \frac{1}{(Q^2 + m_\rho^2)^3} F(x_\rho)\, e^{2\lambda(x_\rho)t}$$

with $x_\rho = \dfrac{Q^2 + m_\rho^2}{2\nu}$, $\nu = (W^2 - m_p^2 + Q^2)/2m_p$, and $F(x_\rho)$, $\lambda(x_\rho)$ being unknown functions.

Differential cross sections, $d\sigma/dt$, for ρ^o production were determined by repeating the fits described above (Eq(9)) for each t interval separately. The results are presented in Fig. 24 together with data from the Cornell experiment[23] corrected as before. For comparison also the photoproduction data of the SBT collaboration[27] are shown. At small momentum transfer, $|t| < 0.4$ GeV^2, the slope A of the t distribution is smaller than at $Q^2 = 0$. Forward cross sections and slope values obtained from exponential fits to $d\sigma/dt$ are listed in Table V.

c) Decay Angular Distributions

The ρ^o decay was analyzed in the s-channel helicity system with the ρ^o cms direction of flight taken as the quantization axis; Θ_H and Φ_H are defined as the polar and azimuthal angles of the decay π^+ in the ρ^o rest frame. The angle between the production plane for $\gamma_V p \to \rho^o p$ and the electron scattering plane (= plane of polarization of the transverse photons) is measured by Φ. In Fig. 25 we show the distribution of $\cos\Theta_H$ and of the polarization angle $\Psi_H = \phi_H - \Phi$ for events in the ρ^o region ($0.60 < M_{\pi^+\pi^-} < 0.85$ GeV). The curves for $W(\cos\Theta_H)$ show the results of the maximum likelihood fits (Eq(9)). At lower W energies the reflection of Δ^{++} production is clearly seen as an accumulation of events near $\cos\Theta_H = -1$. This effect is well accounted for by the fit. The $\cos\Theta_H$ distribution shows that for $W < 2$ GeV more longitudinal ρ^o mesons are produced ($W(\cos\Theta_H) \sim \cos^2\Theta_H$) while for $W > 2$ GeV transverse ρ^o mesons ($W(\cos\Theta_H) \sim \sin^2\Theta_H$) dominate. The Ψ distribution is essentially constant for $W < 2$ GeV but exhibits a strong $\cos^2\Psi$ component at $W > 2$ GeV: like in photoproduction the decay pions are emitted preferentially in the plane of photon polarization.

Since an anisotropic Ψ distribution can only arise from production by transverse photons we see that the ρ^o mesons above $W = 2$ GeV are produced predominantly by transverse photons.

We analyzed the ρ^o decay angular distribution $W(\cos\Theta_H, \phi_H, \Phi)$ in terms of the ρ^o density matrix in the helicity system using the formalism of Ref. 22. The ρ^o density matrix, ρ_{ik}, in general, can be decomposed into seven independent matrices ρ^α_{ik}, $\alpha = 0, \ldots, 6$, where the matrices for $\alpha = 0 - 3$ and 4 describe ρ^o production by transverse and longitudinal photons, respectively; the matrices for $\alpha = 5 - 6$ measure transverse/longitudinal interference terms. When, as in this experiment, the ratio of the longitudinal to transverse photon flux as measured by ε is not varied, the contributions from ρ^o and ρ^4 cannot be separated and $W(\cos,\phi,\Phi)$ measures certain combinations of the ρ^α_{ik}:

$$r^{04}_{ik} = \frac{\rho^{0}_{ik} + \varepsilon R\, \rho^{4}_{ik}}{1 + \varepsilon R}$$

$$r^{\alpha}_{ik} = \frac{\rho^{\alpha}_{ik}}{1 + \varepsilon R} \qquad \alpha = 1\text{-}3$$

$$= \frac{\sqrt{R}\, \rho^{\alpha}_{ik}}{1 + \varepsilon R} \qquad \alpha = 5\text{-}6 \qquad (12)$$

where $R = \sigma_L/\sigma_T$ is the ratio of the cross sections for ρ^0 production by longitudinal and transverse photons. The decay distribution in terms of the r^{α}_{ik} reads (Ref.22):

$$\begin{aligned} W(\cos\theta,\phi,\Phi) = \frac{3}{4\pi} \Big\{ & \frac{1}{2}(1-r^{04}_{00}) + \frac{1}{2}(3r^{04}_{00}-1)\cos^2\theta - \sqrt{2}\ \mathrm{Re}\ r^{04}_{10}\sin 2\theta\cos\phi - r^{04}_{1-1}\sin^2\theta\cos 2\phi \\ & - \varepsilon\cos 2\Phi\{r^{1}_{11}\sin^2\theta + r^{1}_{00}\cos^2\theta - \sqrt{2}\ \mathrm{Re}\ r^{1}_{10}\sin 2\theta\cos\phi - r^{1}_{1-1}\sin^2\theta\cos 2\phi\} \\ & - \varepsilon\sin 2\Phi\{\sqrt{2}\ \mathrm{Im}\ r^{2}_{10}\sin 2\theta\sin\phi + \mathrm{Im}\ r^{2}_{1-1}\sin^2\theta\sin 2\phi\} \\ & + \sqrt{2\varepsilon(1+\varepsilon+\delta)}\ \cos\Phi\{r^{5}_{11}\sin^2\theta + r^{5}_{00}\cos^2\theta - \sqrt{2}\ \mathrm{Re}\ r^{5}_{10}\sin 2\theta\cos\phi - r^{5}_{1-1}\sin^2\theta\cos 2\phi\} \\ & + \sqrt{2\varepsilon(1+\varepsilon+\delta)}\ \sin\Phi\{\sqrt{2}\ \mathrm{Im}\ r^{6}_{10}\sin 2\theta\sin\phi + \mathrm{Im}\ r^{6}_{1-1}\sin^2\theta\sin 2\phi\}\Big\} \end{aligned} \qquad (13)$$

With the exception of r^{04}_{00} the r^{α}_{ik} were determined by the method of moments using all events in the ρ^0 region ($0.60 < M_{\pi\pi} < 0.85$ GeV) at small momentum transfers ($|t| < 0.5$ GeV^2). The element r^{04}_{00}, as mentioned above, was obtained from a maximum likelihood fit to the Dalitz plot distribution (Eq(9)) and is therefore corrected for background effects. Table VI lists the density matrix elements for different W intervals. Also given are the predicted r^{α}_{ik} values if ρ^0 electroproduction conserves the s-channel helicity (SCHC) and proceeds via natural parity exchange only. We conclude from Table VI:

- A certain fraction of the rho mesons is longitudinally aligned (r^{04}_{00} being >0 with 6 s.d.).
- Above W = 2.2 GeV the data show the presence of longitudinal/transverse interference, viz: $\mathrm{Re}\ r^{5}_{10} - \mathrm{Im}\ r^{6}_{10} = 0.182 \pm 0.047 > 0$.

- Those density matrix elements which receive only contributions from helicity flip terms, such as r^{04}_{1o}, r^{04}_{1-1} etc. are small. The measured r^{α}_{ik} values are therefore consistent with the hypothesis that the helicity nonflip amplitudes dominate.

Under the assumption of SCHC we can calculate the longitudinal/transverse ratio

$$R = \frac{1}{\varepsilon} \frac{r^{04}_{oo}}{1 - r^{04}_{oo}} \qquad (14)$$

and find R = 2.2 ± 0.5, 0.43 ± 0.22 and 0.260 ± 0.054 at W ≈ 1.85, 2.1 and 2.45 GeV, respectively, and for an average Q^2 of 0.5 GeV^2. These values are shown in Fig.26 and Table VII together with the results of Ballam at al.[28] and Dakin et al.[29] Fig. 26 suggests that near threshold the ρ^o mesons are produced mainly by longitudinal photons while for W > 2 GeV production by transverse photons dominates. In Fig. 27 the Q^2 dependence of R is given. Themeasurements do not support the hypothesis of Fraas and Schildknecht[24] who conjectured from spin independence $R = \frac{Q^2}{m_\rho^2}$, nor the revised version of Sakurai and Schildknecht[8], namely $R = \xi^2 \frac{Q^2}{m_\rho^2}$ with $\xi^2 \leq 0.12$.

If in addition to SCHC we make the further assumption that the ρ^o mesons are produced by natural parity exchange only, $P = (-1)^J$, we can determine the phase between the production amplitudes for longitudinal and transverse photons:

$$\cos\delta = \frac{1 + \varepsilon R}{\sqrt{R/2}} \cdot \{\mathrm{Re}\ r^5_{1o} - \mathrm{Im}\ r^6_{1o}\} \qquad (15)$$

The resulting phase values are shown in Fig. 26 and Table VII as a function of W together with the result of Refs. 28,29. Fig. 26 suggests that near W = 2.1 GeV both amplitudes are 90° out of phase. With increasing energy the phase difference becomes smaller, being 52 ± 11° at W ≈ 2.5 GeV and 30° → 10° near W = 4.6 GeV, respectively.

5. Omega Production

Omega production

$$\gamma_V p \rightarrow \omega p \tag{16}$$

was studied in the final state

$$ep \rightarrow ep\pi^+\pi^-\pi^o \tag{17}$$

Events selected for reaction (17) had to satisfy the following criteria:

a) they had to give an acceptable kinematical fit to reaction (17) consistent with the ionization observed; b) they did not give an acceptable fit for reaction (8), $ep \rightarrow ep\pi^+\pi^-$. The justification for the last criterion comes from Monte Carlo studies[20] which show that events of reaction (8) may fit reaction (17) but not vice versa.

In the analyzed sample of film were 929 fits for reaction (17) selected in this way with $0.3 < Q^2 < 1.5$ and $W < 2.8$ GeV. The $\pi^+\pi^-\pi^o$ mass distribution is shown in Fig, 28 for different W intervals. At low W's a distinct η signal is observed which presumably stems from the electroproduction of the S_{11} isobar studied recently by Kummer et al.[30] and Beck et al.[31]. The mass distributions above the ω threshold ($W = 1.7$ GeV) show strong ω production. The ω cross section was determined from the mass distributions using hand drawn background curves. The cross section errors include the uncertainty in background subtraction.

The cross section has been corrected for neutral decays, for radiative effects and, taking events with the Monte Carlo programm STYX[20], for losses of ω events into other channels. In Fig. 29 the Q^2 dependence of the ω cross section is given for the W intervals 1.7 - 2.0 and 2.0 - 2.8 GeV. Also shown in Fig. 29 is the VDM prediction (Eq(11)) assuming for ξ^2 the same values as for ρ production. The VDM curves are in reasonable agreement with the data. In Fig. 30 the W dependence of the ratio $\sigma_\omega/\sigma_\rho$ is shown at $\langle Q^2 \rangle = 0.5$ GeV^2 and for photoproduction.[25,32] There is no statistically significant difference between the photo- and electroproduction data.

6. Summary

We have studied hadron production by ep scattering in the kinematical range $0.3 < Q^2 < 1.5$ GeV^2 and $1.3 < W < 2.8$ GeV.

- The average number of charged hadrons, $\langle n \rangle$, produced in an ep collision follows a simple logarithmic law: $\langle n \rangle = (0.79 \pm 0.11) + (0.93 \pm 0.06) \ln(\omega'-1) + (1.04 \pm 0.08) \ln Q^2/m_p^2 \approx 0.8 + \ln s/m_p^2$. It is obvious from this expression and was verified experimentally that $\langle n \rangle$ scales neither with ω' nor with ω_W.
- A ~10 % decrease of $\langle n \rangle$ between $Q^2 = 0$ and ~1 GeV^2 for $W > 1.8$ GeV was traced back to an increase of the channels with one-charged hadron in the final state and a reduction of the three-charged hadron production (e.g. $\gamma_V p \to \rho^o p$).
- Inclusive π^- production was analyzed in terms of $(x, p_\perp^2)$ and (M_X, t) with respect to Q^2, W and Q^2, ω'.
  The normalized invariant π^- cross section, $F(x)$, for fixed W shows no Q^2 dependence in the target fragmentation and central region. In the beam fragmentation region ($x \gtrsim 0.3$) the π^- yield is reduced by a factor of 1.5 - 2.0 compared to photoproduction. Most of this effect can be understood in terms of the smaller ρ^o cross section in electroproduction. The transverse momentum distributions for fixed W show no Q^2 dependence.
- For fixed ω', $F(x)$ was found to increase with Q^2 in the central region, i.e. $F(x)$ does not scale with respect to ω' in our kinematical range.
- For fixed ω', the slope of the $p_\perp^2$ distribution decreases with Q^2. This decrease is most pronounced (by a factor of two between $Q^2 \sim 0.5$ and 1 GeV^2) in the so called non diffractive region, $2.5 < \omega' < 6$ and for $6 < \omega' < 10$. In the diffractive region, $10 < \omega' < 15$, the effect is small.
- For π^- in the forward hemisphere, $x > 0$, the average transverse momentum is found to increase with Q^2 like the average longitudinal momentum.
- The distribution of the angle Φ between the electron scattering and π^- production plane is found to be approximately constant in the target fragmentation and central region.

- In the beam fragmentation region a fit to the Φ distribution yielded $W(\Phi) = 1 + (0.40 \pm 0.09)\ \varepsilon\cos 2\Phi - (0.23 \pm 0.05)\ \sqrt{2\varepsilon(\varepsilon+1)}\cos\Phi$ which establishes the presence of a longitudinal/transverse interference term. A part of the observed Φ anisotropy is due to π^- mesons from ρ^o production, $\gamma_V p \to \rho^o p$.

- The Q^2 dependence of the ρ^o cross section, $\sigma(\gamma_V p \to \rho^o p)$, for $W > 2$ GeV is essentially determined by the ρ propagator as suggested by VDM.

- The slope of the differential cross section, $d\sigma/dt$, for ρ^o production measured at an average Q^2 of 0.4 GeV^2 is smaller than observed for photoproduced ρ^o mesons.

- The ρ^o polar decay angular distribution in the helicity system shows a nonzero longitudinal part, r^{04}_{oo} being 0.183 ± 0.031 for W between 2.2 and 2.8 GeV. The distribution of the angle ψ, sensitive to linear photon polarisation exhibits a strong $\cos^2\psi$ component at $W > 2.2$ GeV and demonstrates that the ρ^o mesons are produced predominantly by transverse photons.

- The results presented for the ρ^o density matrix elements suggest that s-channel helicity flip amplitudes are small compared to non flip amplitudes. Assuming s-channel helicity conservation we find for ρ^o production $R = \sigma_L/\sigma_T = 0.260 \pm 0.054$ for $\langle W \rangle = 2.45$ and $\langle Q^2 \rangle = 0.5$ GeV^2.

  The density matrix elements for $W > 2.2$ GeV show the existence of an interference between production by longitudinal and transverse photons. Assuming SCHC and only natural parity exchange, the phase between the two amplitudes is found to be $\cos\delta = 0.61 \pm 0.15$ for $\langle W \rangle = 2.45$ GeV and $\langle Q^2 \rangle = 0.5$ GeV^2.

  A pronounced ω peak is observed in the $\pi^+\pi^-\pi^o$ mass distribution for the process $\gamma_V p \to p\pi^+\pi^-\pi^o$. The cross section for $\gamma_V p \to \omega p$ is given as a function of Q^2 and W.

Acknowledgements

We wish to thank Prof. E. Lohrmann and Prof. M.W. Teucher for their encouragement. Many people have helped to make this experiment possible. We are indebted to N. Gollmer, V. Heynen, A. Huber, K. Klinkmüller, G. Kraft, H.H. Sabath, H.W. Sass, K. Westphal, K.H. Wroblewski, and Mrs. Hell for technical assistence. We are grateful to Dr. Horlitz and his group for their help with the streamer chamber magnet. The excellent performance of the Synchrotron crew, of the Hallendienst and of the Kältetechnik is gratefully acknowledged. We want to thank our scanning and measuring personnel for their painstaking work. The cooperation by Mr. Kuhlmann and the Rechenzentrum has been invaluable.

List of References

1. A preliminary version of this paper has been contributed to the International Symposium on Electron and Photon Interactions at High Energies, Bonn, 1973

2. V. Eckardt et al., Nucl. Phys. B55, 45 (1973).

3. L. Hand, Phys. Rev. 129, 1834 (1963).

4. F.W. Brasse et al., Nuovo Cimento 55A, 679 (1968);
W. Albrecht et al., Nucl. Phys. B13,1 (1969).

5. G. Miller et al., Phys. Rev. D5, 528 (1972).

6. J. Moritz et al., Nucl. Phys. B41, 336 (1972), DESY Report 71/61 (1971).

7. F.W. Brasse et al., Nucl. Phys. B39, 421 (1972).

8. J.J. Sakurai and D. Schildknecht, Phys. Letters 40B, 121 (1972).
J.J. Sakurai, Erice Lectures, 1973 and UCLA preprint.

9. A. Bramon, E. Etim and M. Greco, Phys. Letters 41B, 609 (1972);
M. Greco, CERN Report TH-1617 (1973).

10. J. Ballam et al., Contribution to the Symposium cited in Ref. 1; see Ref.11.

11. F.W. Brasse, rapporteur's talk ibid. DESY Report 73/49 (1973).

12. K.C. Moffeit et al., Phys. Rev. D5, 1603 (1972).

13. C. Driver et al., Phys. Letters 35B, 81 (1971) ; Nucl. Phys. B30, 245 (1971);
C.N. Brown et al., Phys. Rev. Letters 26, 987 (1971).

14. S.D. Drell, D.J. Levy and T.M. Yan, Phys. Rev. Letters 22, 744 (1969).

15. T.T. Chou and C.N. Yang, Phys. Rev. D4, 2004 (1971).

16. J. Bjorken, Proceedings of the 1971 International Symposium on Electron and Photon Interactions at High Energies, ed. by N.B. Mistry (Cornell University, Ithaca), p.281.

17. K. Berkelman et al., CORNELL Report CLNS 240 (1973), data cited by F.W. Brasse, Ref. 11.

18. See e.g. F. Gutbrod and E.E. Schröder, DESY Report 73/14 (1973).

19. N.S. Craigie, G. Kramer and J. Körner, Inclusive Photo- and Electroproduction of Pions, in the Triple Regge Region, DESY Report 73/35 (1973).

20. H. Nagel and K. Wacker, STYX, computer code to simulate streamer chamber events, Hamburg, 1973.

21. G. Drews, MLHFIT, computer code, Hamburg 1973.

22. K. Schilling and G. Wolf, Nucl. Phys. B61, 381 (1973).

23. L. Ahrens et al., Phys. Rev. Letters 31, 131 (1973).

24. H. Fraas and D. Schildknecht, Nucl. Phys. B14, 543 (1969).

25. Aachen-Berlin-Bonn-Hamburg-Heidelberg-München Collaboration, Phys. Rev. 175, 1669 (1968).

26. G. Preparata, University of Rome preprint, 1973.

27. SLAC-Berkely-Tufts Collaboration, Phys. Rev. D5, 545 (1972).

28. J. Ballam et al., Contribution to the Symposium cited in Ref. 1; see also the rapporteurs talk of K. Moffeit, SLAC-PUB-1314 and R. Talman at this conference.

29. J.T. Dakin et al., Phys. Pev. Letters 30, 142 (1973).

30. P.S. Kummer et al., Phys. Rev. Letters 30, 873 (1973).

31. U. Beck et al., Contribution to the Symposium in Ref. 1.

32. SLAC-Berkeley Collaboration, Phys. Rev. D7, 3150 (1973).

Table I: Mean values of the variables W, Q^2, ω', ω_W for the various kinematical regions used in this paper

	Kinematical regions			Mean values			
W (GeV)	Q^2 (GeV^2)	ω'	ω_W	$\langle W \rangle$	$\langle Q^2 \rangle$	$\langle \omega' \rangle$	$\langle \omega_W \rangle$
1.5 - 1.8	0.3 - 0.5	no cut	no cut	1.65	0.39	8.2	
	0.5 - 0.8				0.63	5.4	
	0.8 - 1.5				1.00	3.8	
	0.5 - 1.5				0.77	4.8	
1.8 - 2.2	0.3 - 0.5			2.0	0.39	11.1	
	0.5 - 0.8				0.63	7.4	
	0.8 - 1.5				1.01	4.9	
	0.5 - 1.5				0.79	6.4	
2.2 - 2.8	0.3 - 0.5			2.5	0.42	11.0	
	0.5 - 0.8				0.62	7.0	
	0.8 - 1.5				1.07	5.1	
	0.5 - 1.5				0.79	9.5	
1.7 - 2.0	0.3 - 0.5			1.8	0.40	9.6	
	0.5 - 0.8				0.61	6.6	
	0.8 - 1.5				1.05	4.4	
2.0 - 2.2	0.3 - 0.5			2.1	0.40	12.2	
	0.5 - 0.8				0.62	8.2	
	0.8 - 1.5				1.01	5.4	
1.8 - 2.8	0.3 - 0.5			2.2	0.40	13.1	
	0.5 - 0.8				0.62	9.4	
	0.8 - 1.5				1.04	6.0	
	0.5 - 1.5				0.79	7.9	
1.3 - 2.8	0.3 - 0.7	2.5 - 6.0	"	1.5	0.54	5.1	
	0.7 - 1.0			1.7	0.84	4.5	
	1.0 - 1.5			1.9	1.21	4.0	
	0.3 - 1.0			1.6	0.68	4.8	
	0.3 - 0.5	6 - 10		1.6	0.39	7.8	
	0.5 - 0.7			2.0	0.60	7.8	
	0.7 - 1.5			2.4	0.91	7.6	
	0.3 - 0.7			1.7	0.45	7.8	
	0.3 - 0.5	10 - 15		2.1	0.38	12.1	
	0.5 - 0.7			2.5	0.57	11.9	
	0.7 - 1.5			2.7	0.76	10.6	
	0.5 - 1.5			2.5	0.59	11.8	
	0.3 - 0.5	no cut	2.5 - 4	1.4	0.39		3.6
	0.5 - 0.7			1.5	0.60		3.4
	0.7 - 1.5			1.7	0.95		3.3
	0.3 - 0.5		4 - 6	1.7	0.38		4.9
	0.5 - 0.7			2.0	0.59		4.9
	0.7 - 1.5			2.3	0.97		4.9
	0.3 - 0.5		6 - 8	2.2	0.39		6.9
	0.5 - 0.7			2.4	0.59		6.9
	0.7 - 1.5			2.6	0.83		6.7
	0.3 - 0.5		8 - 15	2.6	0.42		9.0
	0.5 - 0.7			2.7	0.56		8.5

Table II: Results of exponential fits $C \exp(-Ap_\perp^2)$ to $p_\perp^2$-distributions for inclusive π^- production as a function of W and Q^2

	W (GeV)	Q^2 (GeV^2)	$C=\frac{1}{\pi\sigma_{tot}}\frac{d\sigma}{dp_\perp^2 dx}\Big\vert_{p_\perp^2=0}$ (GeV)$^{-2}$	A (GeV^{-2})
$-0.2 < x < 0.2$	1.5 - 1.8	0.3 - 0.5	0.93 ± 0.20	14.4 ± 3.2
		0.5 - 1.5	0.84 ± 0.13	14.1 ± 1.9
	1.8 - 2.2	0.3 - 0.5	1.11 ± 0.16	13.9 ± 1.5
		0.5 - 1.5	0.83 ± 0.10	9.0 ± 1.1
	2.2 - 2.8	0.3 - 0.5	0.98 ± 0.07	9.0 ± 0.7
		0.5 - 1.5	0.94 ± 0.07	8.1 ± 0.7
$0.3 < x < 0.7$	1.5 - 1.8	0.3 - 0.5	0.53 ± 0.15	15.2 ± 3.6
		0.5 - 1.5	0.52 ± 0.11	9.7 ± 2.0
	1.8 - 2.2	0.3 - 0.5	0.33 ± 0.08	5.7 ± 1.6
		0.5 - 1.5	0.36 ± 0.07	8.0 ± 1.5
	2.2 - 2.8	0.3 - 0.5	0.40 ± 0.07	8.2 ± 1.3
		0.5 - 1.5	0.39 ± 0.07	8.8 ± 1.3

Table III: Results of exponential fits $C \exp(-Ap_\perp^2)$ to $p_\perp^2$-distributions for inclusive π^- production as a function of ω' and Q^2

	ω'	Q^2 (GeV^2)	$C = \frac{1}{\sigma_{tot}} \frac{d\sigma}{dp_\perp^2 dx}\Big\|_{p_\perp^2=0}$ (GeV^{-2})	A (GeV^{-2})
$-0.2 < x < 0.2$	2.5 - 6	0.3 - 1.0	0.80 ± 0.13	16.7 ± 2.3
		1.0 - 1.5	0.86 ± 0.15	9.8 ± 1.7
	6 - 10	0.3 - 0.7	1.07 ± 0.13	14.3 ± 1.1
		0.7 - 1.5	0.92 ± 0.10	7.0 ± 0.9
	10 - 15	0.3 - 0.5	0.86 ± 0.11	10.6 ± 1.1
		0.5 - 1.5	0.85 ± 0.09	8.3 ± 1.0
$0.3 < x < 0.7$	2.5 - 6	0.3 - 1.0	0.39 ± 0.08	9.8 ± 1.6
		1.0 - 1.5	0.43 ± 0.14	5.5 ± 3.5
	6 - 10	0.3 - 0.7	0.43 ± 0.08	10.6 ± 1.5
		0.7 - 1.5	0.44 ± 0.12	9.6 ± 2.4
	10 - 15	0.3 - 0.5	0.44 ± 0.08	8.8 ± 1.4
		0.5 - 1.5	0.31 ± 0.08	5.3 ± 2.0

Table IV: Reaction $\gamma_V p \to p\pi^+\pi^-$

Percentages $a_{\Delta^{++}}$, a_{Δ^o}, a_ρ of Δ^{++}, Δ^o and ρ^o production and the ρ^o density matrix element r_{oo}^{o4} as obtained from the maximum likelihood fits to the Dalitz plot density.

W (GeV)	Q^2 (GeV^2)	Number of events	$a_{\Delta^{++}}$	a_{Δ^o}	a_ρ	r_{oo}^{o4}
1.7 - 2.0	0.3 - 1.5	670	0.236 ± 0.036	0	0.343 ± 0.036	0.676 ± 0.054
	0.3 - 0.5	332	0.240 ± 0.052	0	0.298 ± 0.070	0.676
	0.5 - 0.8	242	0.280 ± 0.061	0.045 ± 0.025	0.403 ± 0.075	0.676 } fixed
	0.8 - 1.5	96	0.177 ± 0.094	0	0.300 ± 0.119	0.676
2.0 - 2.2	0.3 - 1.5, $\cos\Theta^*_{\pi^+\pi^-} > 0.75$	111	0.137 ± 0.052	0.001 ± 0.006	0.645 ± 0.105	0.284 ± 0.103
	0.3 - 1.5	270	0.218 ± 0.043	0.017 ± 0.014	0.353 ± 0.064	0.284
	0.3 - 0.5	153	0.350 ± 0.060	0.050 ± 0.030	0.326 ± 0.080	0.284 } fixed
	0.5 - 0.8	84	0.040 ± 0.043	0	0.365 ± 0.114	0.284
	0.8 - 1.5	33	0.090 ± 0.088	0	0.535 ± 0.200	0.284
2.2 - 2.8	0.3 - 1.5, $\cos\Theta^*_{\pi^+\pi^-} > 0.75$	199	0.191 ± 0.034	0.063 ± 0.022	0.701 ± 0.041	0.183 ± 0.031
	0.3 - 1.5	339	0.139 ± 0.029	0.028 ± 0.014	0.441 ± 0.043	0.183
	0.3 - 0.5	165	0.150 ± 0.043	0.038 ± 0.025	0.543 ± 0.060	0.183 } fixed
	0.5 - 0.8	133	0.156 ± 0.046	0.037 ± 0.026	0.388 ± 0.069	0.183
	0.8 - 1.5	41	0.074 ± 0.044	0	0.218 ± 0.108	0.183

Table V: Reaction $\gamma_V p \to \rho^o p$. Cross sections and fraction of the total cross section together with the modification for $|t|_{min}$ cutoff; fit parameters of $d\sigma/dt$ to the form $d\sigma^o/dt \exp At$ for $|t| < 0.4$ GeV^2. The photoproduction data have been taken from Refs. 24,25. For the total virtual photon proton cross section, $\sigma_{tot} = \sigma_T + \varepsilon\sigma_L$ we use the values obtained in this experiment.

W (GeV)	Q^2 (GeV^2)	σ_ρ (μb)	σ_ρ/σ_{tot}	$\sigma_\rho/\sigma_{tot} e^{A\|t\|_{min}}$	$d\sigma^o/dt$ (μb GeV^{-2})	A (GeV^{-2})
1.7 - 2.0	0	20.0 ± 1.2	0.13 ± 0.01			
	0.3 - 0.5	10.2 ± 2.4	0.078 ± 0.020			
	0.5 - 0.8	10.3 ± 1.9	0.154 ± 0.031			
	0.8 - 1.5	6.4 ± 2.5	0.156 ± 0.066			
2.0 - 2.2	0	24.8 ± 1.4	0.17 ± 0.01			
	0.3 - 0.5	6.0 ± 1.5	0.090 ± 0.023			
	0.5 - 0.8	5.1 ± 1.6	0.103 ± 0.034			
	0.8 - 1.5	5.4 ± 2.0	0.111 ± 0.044			
2.2 - 2.8	0	18.4 ± 0.6	0.160 ± 0.008	0.186 ± 0.009	148.2 ± 6.7	6.25 ± 0.20
	0.3 - 0.5	4.2 ± 0.5	0.051 ± 0.006	0.058 ± 0.007	26.5 ± 5.5	5.5 ± 1.1
	0.5 - 0.8	3.2 ± 0.6	0.048 ± 0.009	0.060 ± 0.011	14.0 ± 3.4	4.9 ± 1.3
	0.8 - 1.5	0.84± 0.42	0.019 ± 0.010	0.029 ± 0.015		

Table VI: ρ^o-density matrix elements in the helicity system from events of the reaction $\gamma_V p \to \pi^+\pi^- p$ in the ρ^o region (0.60 - 0.86 GeV), for $|t| < 0.5$ GeV^2 and $\langle Q^2 \rangle = 0.5$ GeV^2. For comparison the density matrix elements as predicted for SCHC and natural parity exchange only.

	W:1.7-2.0 GeV	W:2.0-2.2 GeV	W:2.2-2.8 GeV	Prediction with SCHC and R=0.3
r^{04}_{oo} *	0.676±0.054	0.284±0.103	0.183±0.031	
Re r^{04}_{1o}	0.060±0.026	0.157±0.050	0.065±0.042	0
r^{04}_{1-1}	-0.045±0.036	0.019±0.084	-0.080±0.065	0
r^{1}_{oo}	-0.004±0.064	-0.172±0.142	0.092±0.107	0
r^{1}_{11}	0.014±0.033	-0.035±0.090	-0.095±0.084	0
Re r^{1}_{1o}	-0.024±0.037	-0.238±0.077	0.097±0.066	0
r^{1}_{1-1}	0.062±0.054	0.233±0.126	0.357±0.105	0.39
Im r^{2}_{1o}	-0.011±0.036	-0.123±0.079	0.004±0.060	0
Im r^{2}_{1-1}	0.049±0.056	-0.082±0.114	-0.279±0.097	-0.39
r^{5}_{oo}	-0.003±0.033	0.134±0.073	-0.015±0.054	0
r^{5}_{11}	0.037±0.016	-0.026±0.044	-0.030±0.040	0
Re r^{5}_{1o}	0.007±0.019	-0.041±0.044	0.095±0.034	0.15 cosδ
r^{5}_{1-1}	-0.030±0.027	0.048±0.065	-0.018±0.053	0
Im r^{6}_{1o}	-0.016±0.018	-0.045±0.038	-0.087±0.031	-0.15 cosδ
Im r^{6}_{1-1}	0.077±0.027	0.109±0.052	0.040±0.050	0

* Determined by a maximum likelihood fit to the Dalitz plot density (see text) and therefore corrected for background contributions

Table VII: $\gamma_V p \to \rho^o p$: Density matrix elements, $R = \sigma_L/\sigma_T$ and $\cos\delta$ calculated under the assumption of SCHC and natural parity exchange only.

W (GeV)	Q^2 (GeV^2)	$\langle\varepsilon\rangle$	r^{o4}_{oo}	R	Re r^5_{1o} - Im r^6_{1o}	$\cos\delta$
1.7 - 2.0	0.3 - 1.5	0.96	0.676 ± 0.054	2.20 ± 0.54	0.023 ± 0.026	0.067 ± 0.08
2.0 - 2.2	0.3 - 1.5	0.93	0.284 ± 0.103	0.43 ± 0.22	0.004 ± 0.058	0.012 ± 0.18
2.2 - 2.8	0.3 - 1.5	0.86	0.183 ± 0.031	0.260 ± 0.054	0.182 ± 0.045	0.61 ± 0.15
2.2 - 2.8	0.3 - 0.5		0.152 ± 0.062	0.196 ± 0.097		
	0.5 - 0.8		0.308 ± 0.120	0.495 ± 0.280		
	0.8 - 1.5		0.345 ± 0.228	0.590 ± 0.590		

Figure Captions

1. Total electroproduction cross section, σ_{tot}, as a function of Q^2 for various W intervals. Our data are compared with those of other experiments.[4-6]

2. Average multiplicity of charged hadrons, $\langle n \rangle$:
   a) for different W intervals as a function of Q^2
   b) for different Q^2 intervals as a function of s together with preliminary data from SLAC[10].
   The $Q^2 = 0$ data were taken from Ref. 11.

3. Relative contribution of reactions with $\langle n \rangle$ charged hadrons (n = 1, 3, 5) to the total cross section. The $Q^2 = 0$ points stem from Ref. 4. The curves are drawn to guide the eye.

4.a) $\langle n \rangle$ as a function of Q^2 for fixed ω' intervals. The lines are fits to the expression $\langle n \rangle = C_o + C_\omega \ln(\omega'-1) + C_Q \ln Q^2/m_p^2$ (see text).
   b) $\langle n \rangle$ as a function of ω' for fixed Q^2 intervals.

5. Toplogical cross sections as a function of Q^2 for fixed ω' intervals. The curves are drawn to guide the eye.

6.a) $\langle n \rangle$ for different Q^2 intervals as a function of ω_W.
   b) $\langle n \rangle$ for different ω_W intervals as a function of Q^2.

7.a-c) Normalized structure function F(x) for inclusive π^- electroproduction for different W,Q^2 intervals.
   d) F(x) for inclusive π^- electroproduction after removal of the ρ^o contribution ($0.6 < M_{\pi^+\pi^-} < 0.9$ GeV in the reaction $\gamma_V p \to \pi^+\pi^- p$) for different Q^2 intervals in the W region 2.2 - 2.8 GeV.
   The curves in Figs. 7d,c show the $Q^2 = 0$ result (Ref. 12).

8. Normalized structure function, $F(x,p^2)$, for inclusive π^- production averaged over the x intervals (-0.2 - 0.2) and 0.3 - 0.7, respectively. for different Q^2 and W intervals. The straight lines show the result from exponential fits to the form $C \exp(-Ap^2)$.

9. Rapidity distributions for inclusive π^- production for different W and Q^2 intervals.

10. $F(x)$ for inclusive π^- production for different ω' and Q^2 bins.

11. $F(x,p_\perp^2)$ for inclusive π^- production for different ω' and Q^2 intervals in the two x regions (-0.2) - 0.2 and 0.3 - 0.7. The straight lines show the result from fits to the form C exp $(-Ap_\perp^2)$.

12. Average π^- transverse and longitudinal momenta, $\langle p_\perp \rangle$ and $\langle p_{\parallel} \rangle$, in the x interval 0 - 1.0 as a function of Q^2 for fixed ω'.

13. Normalized cross section $\frac{1}{\pi\sigma_{tot}} \frac{d\sigma}{dM_X}$ (M_X = missing mass in the reaction $\gamma_V p \to \pi^- X$) for fixed W,Q^2 intervals.

14. Normalized cross section $\frac{1}{\pi\sigma_{tot}} \frac{d\sigma}{dM_X}$ (M_X = missing mass in the reaction $\gamma_V p \to \pi^- X$) for fixed ω',Q^2 intervals.

15. Chew-Low plot of the four momentum transfer t_{γ_V/π^-} versus missing mass M_X in the W interval 1.8 - 2.8 GeV for $0.3 < Q^2 < 1.5$ GeV^2. For bin contents larger or equal to 10, letters are being used: A,B,C,... correspond to 11,12,13,....

16. $\frac{1}{\pi\sigma_{tot}} \frac{d\sigma}{dt_{\gamma_V/\pi^-}}$ for different M_X and Q^2 intervals. The curves are drwan to guide the eye.

17. x versus Φ for inclusive π^- production from $1.8 < W < 2.8$ GeV and $0.3 < Q^2 < 1.5$ GeV^2. Φ is the angle between the electron scattering plane and the π^- production plane.

18. Φ versus W for inclusive π^- production

    a) for the central region, $-0.2 < x < 0.2$

    b) for the beam fragmentation region, $0.3 < x < 0.7$.

19. $W(\Phi)$ for inclusive π^- production in the central region for $1.8 < W < 2.8$ GeV and different Q^2 intervals.

20. $W(\Phi)$ for inclusive π^- production in the beam fragmentation region for $1.8 < W < 2.8$ GeV and $0.3 < Q^2 < 1.5$ GeV^2.

a) all events. The curve shows the result of a fit to the form (see text)

$$W(\Phi) = 1 + \varepsilon C_p \cos 2\Phi + \sqrt{2\varepsilon(\varepsilon+1)}\, C_I \cos\Phi$$

b) for events without ρ^o (⊕) and for ρ^o events alone (⊖).

21. Reaction $\gamma_V p \to p\pi^+\pi^-$: $p\pi^+$, $\pi^+\pi^-$ and $p\pi^-$ mass distributions for $1.7 < W < 2.0$ GeV and different Q^2 intervals. The curves show the results of the maximum likelihodd fits (see text).

22. Reaction $\gamma_V p \to p\pi^+\pi^-$: $p\pi^+$, $\pi^+\pi^-$ and $p\pi^-$ mass distributions for $2.0 < W < 2.2$ GeV and $2.2 < W < 2.8$ GeV with $0.3 < Q^2 < 1.5$ GeV^2. The curves show the results of the maximum likelihood fits (see text). ▨ $M(\pi^+\pi^-)$ for forward produced $(\pi^+\pi^-)$ systems: $\cos\Theta^{CMS}_{\pi^+\pi^-} > 0.75$.

23. Reaction $\gamma_V p \to \rho^o p$: Total cross section as a function of Q^2 for different W intervals determined in this experiment (o). From the data of Ahrens et al.[23] the ω contribution is subtracted (x). The values at $Q^2 = 0$ have been measured by the ABBHHM Collaboration[25]. The curve labelled VDM was calculated according to Eq(11).

24. Reaction $\gamma_V p \to \rho^o p$: Differential cross section, $d\sigma/dt$, (t = square of the four momentum transfer between the incoming and outgoing proton) for $2.2 < W < 2.8$ GeV , $0.3 < Q^2 < 0.5$ GeV^2 and $0.5 < Q^2 < 1.5$ GeV^2 (⊕). The cross sections were obtained by maximum likelihood fits (see text). From the data of Ahrens et al.[23] the ω contribution is subtracted (x). The open points (⊖) show the photoproduction data of the SBT collaboration[27].

25. Reaction $\gamma_V p \to \rho^o p$: Decay angular distributions in the helicity system for events in the ρ^o region ($0.6 < M_{\pi\pi} < 0.85$ GeV). The curves show the results of the maximum likelihood fits (see text).

26. Reaction $\gamma_V p \to \rho^o p$: Density matrix element r^{04}_{oo}, $R = \sigma_T/\sigma_L$ (Eq(14)) and $\cos\delta$ (Eq(15)) as a function of W for $\langle Q^2\rangle = 0.5$ GeV^2. For details see text.

27. Reaction $\gamma_V p \to \rho^o p$: $R = \sigma_T/\sigma_L$ as a function of Q^2 for $2.0 < W < 2.8$ GeV (⧳). Results from Ballam et al.[28] (x) and Dakin et al.[29] (⧲) are also shown. The curves show predictions from vector dominance models.[24]

28. Reaction $\gamma_V p \to p\pi^+\pi^-\pi^o$: $\pi^+\pi^-\pi^o$ mass-distribution for various W and Q^2 intervals.

29. Reaction $\gamma_V p \to \omega p$: Total cross section as a function of Q^2 for the W intervals 1.7 - 2.0 and 2.0 - 2.8 GeV. Corrections for neutral decays, radiative effects and experimental losses have been applied. The curve labelled VDM was calculated according to Eq(11).

30. The ratio of ω to ρ^o cross sections, $\sigma_{\omega p}/\sigma_{\rho^o p}$ as a function of W for $\langle Q^2 \rangle = 0.5$ GeV^2 (⧳). Photoproduction data are taken from the ABBHHM Collaboration[25] (⧲) and the SBT Collaboration[32] (⧲).

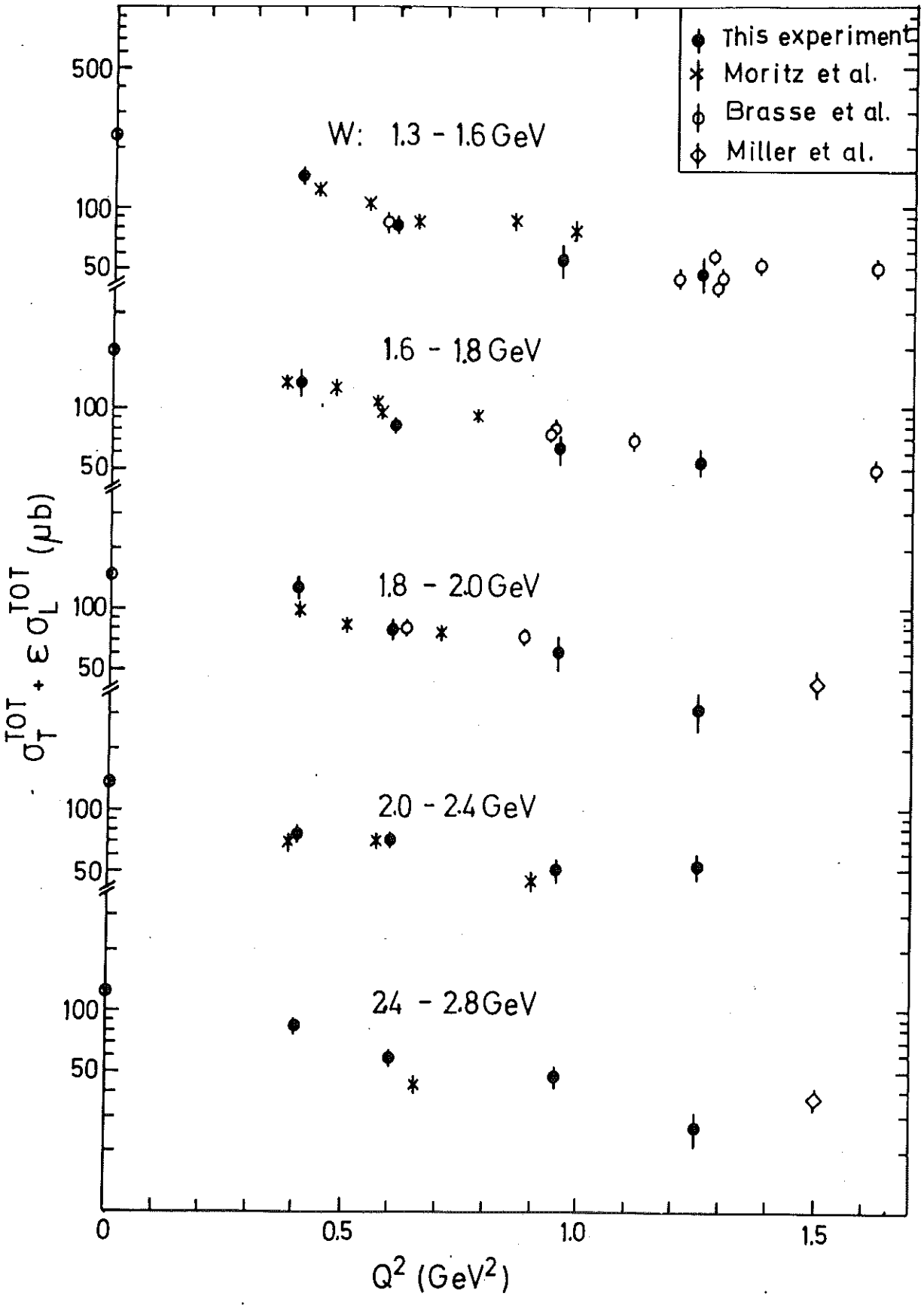
This experiment
Moritz et al.
Brasse et al.
Miller et al.
W: 1.3 - 1.6 GeV
1.6 - 1.8 GeV
1.8 - 2.0 GeV
2.0 - 2.4 GeV
2.4 - 2.8 GeV
500
100
50
0
0.5
1.0
1.5
$\sigma_T^{TOT} + \varepsilon \sigma_L^{TOT}$ (μb)
Q^2 (GeV^2)

Fig. 1

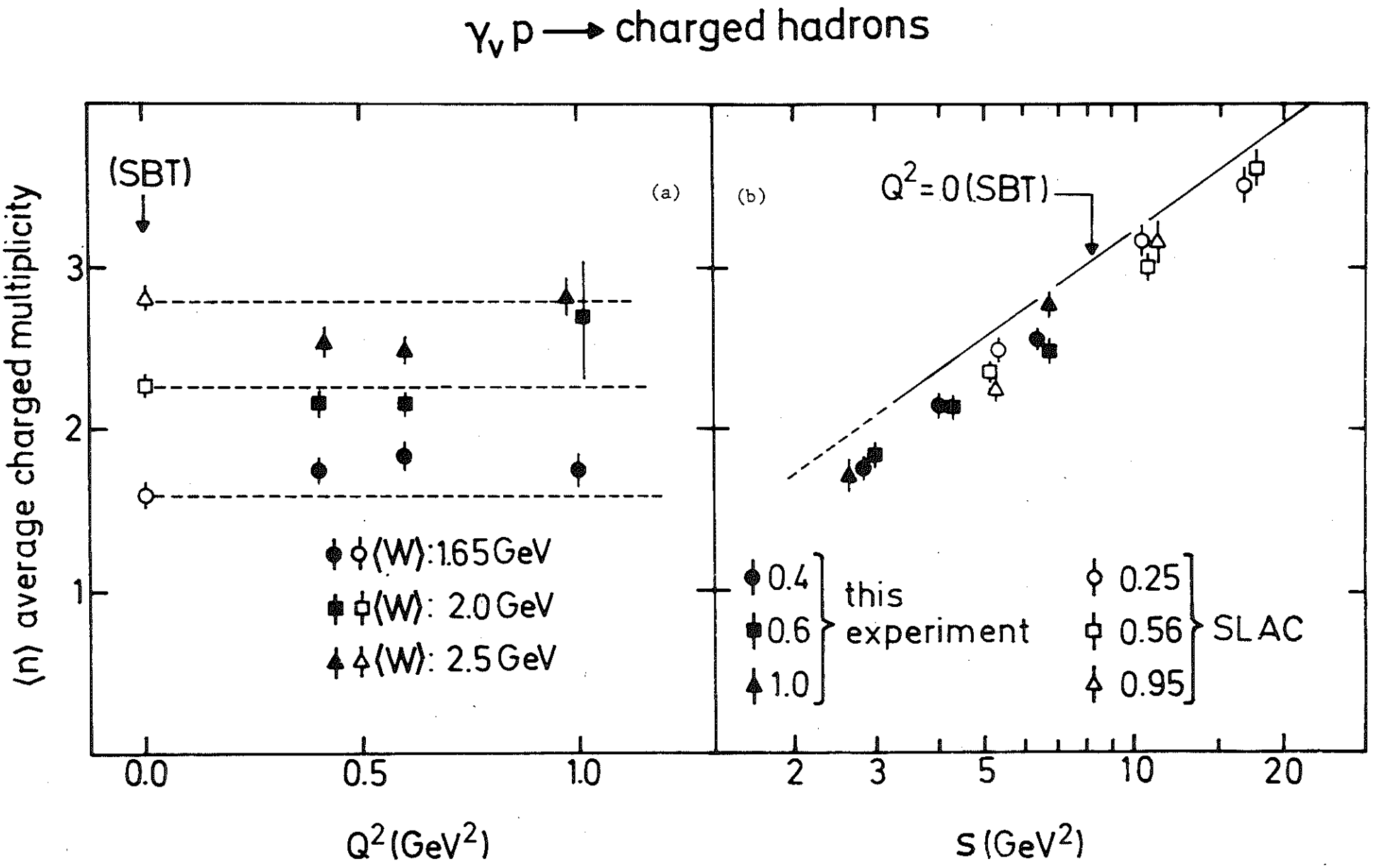
$\gamma_v p \longrightarrow$ charged hadrons
(SBT)
(a)
(b)
$Q^2 = 0$ (SBT)
⟨n⟩ average charged multiplicity
⟨W⟩: 1.65 GeV
⟨W⟩: 2.0 GeV
⟨W⟩: 2.5 GeV
0.4
0.6
1.0
this experiment
0.25
0.56
0.95
SLAC
0.0
0.5
1.0
2
3
5
10
20
Q^2 (GeV^2)
s (GeV^2)

Fig.2

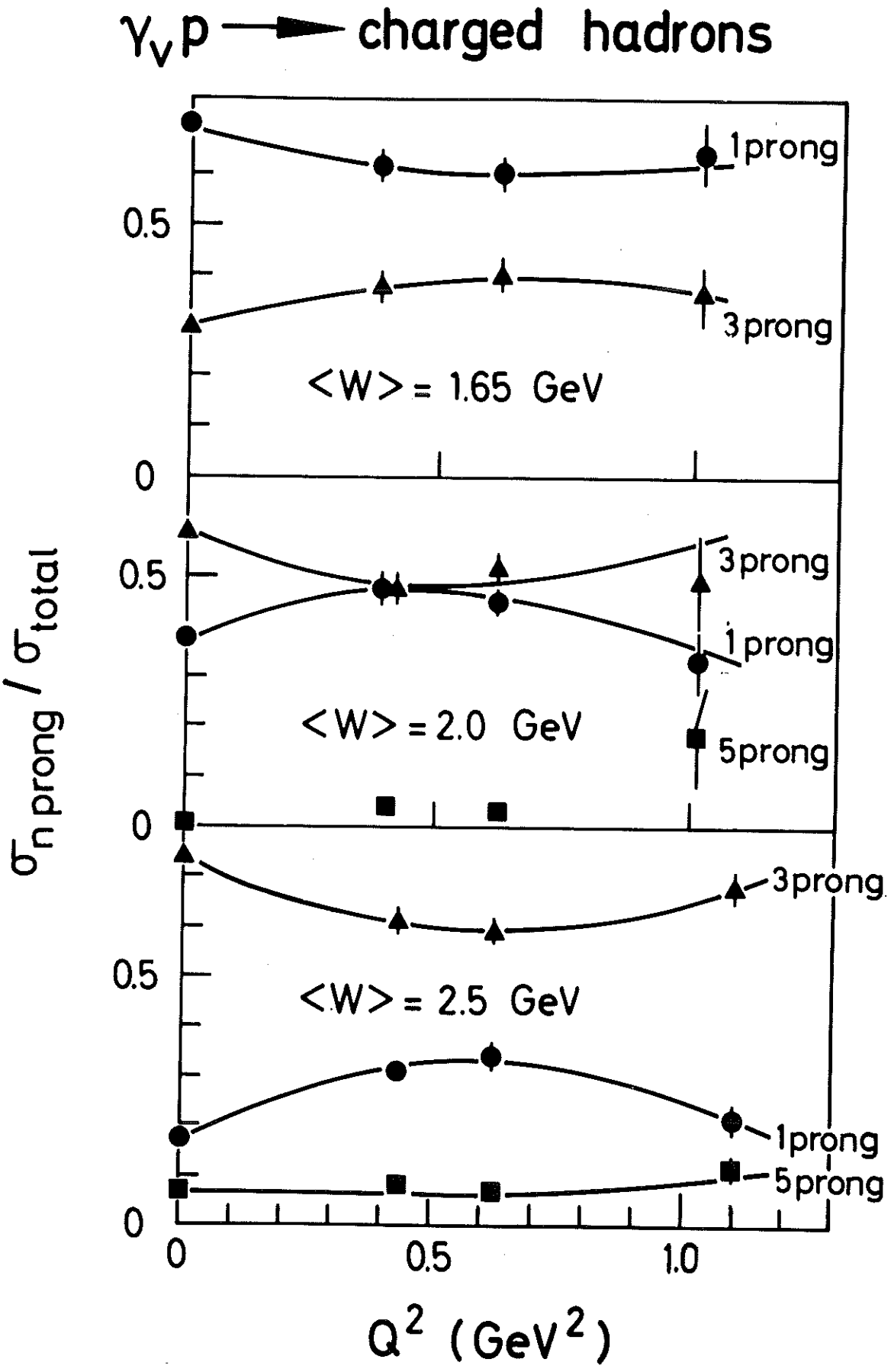
$\gamma_V p \longrightarrow$ charged hadrons
1prong
3prong
<W> = 1.65 GeV
3prong
1prong
5prong
<W> = 2.0 GeV
3prong
<W> = 2.5 GeV
1prong
5prong
0.5
0
0.5
0
0.5
0
0
0.5
1.0
$\sigma_{n\,prong} / \sigma_{total}$
Q^2 (GeV^2)

Fig. 3

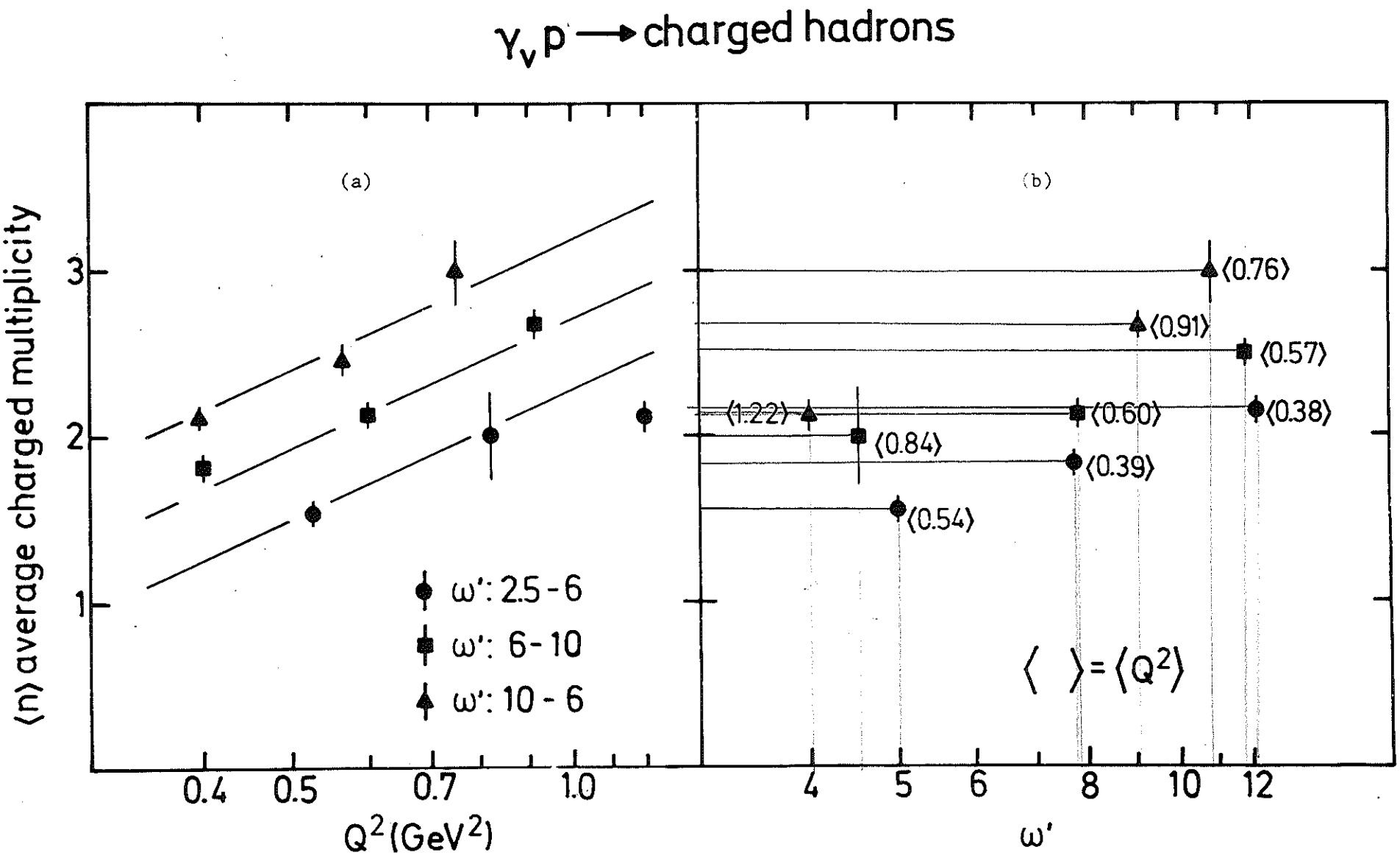
$\gamma_v p \longrightarrow$ charged hadrons
(a)
(b)
⟨n⟩ average charged multiplicity
3
2
1
ω': 2.5 - 6
ω': 6 - 10
ω': 10 - 6
0.4
0.5
0.7
1.0
Q^2 (GeV^2)
⟨0.76⟩
⟨0.91⟩
⟨0.57⟩
⟨1.22⟩
⟨0.60⟩
⟨0.38⟩
⟨0.84⟩
⟨0.39⟩
⟨0.54⟩
⟨ ⟩ = ⟨Q^2⟩
4
5
6
8
10
12
ω'

Fig.4

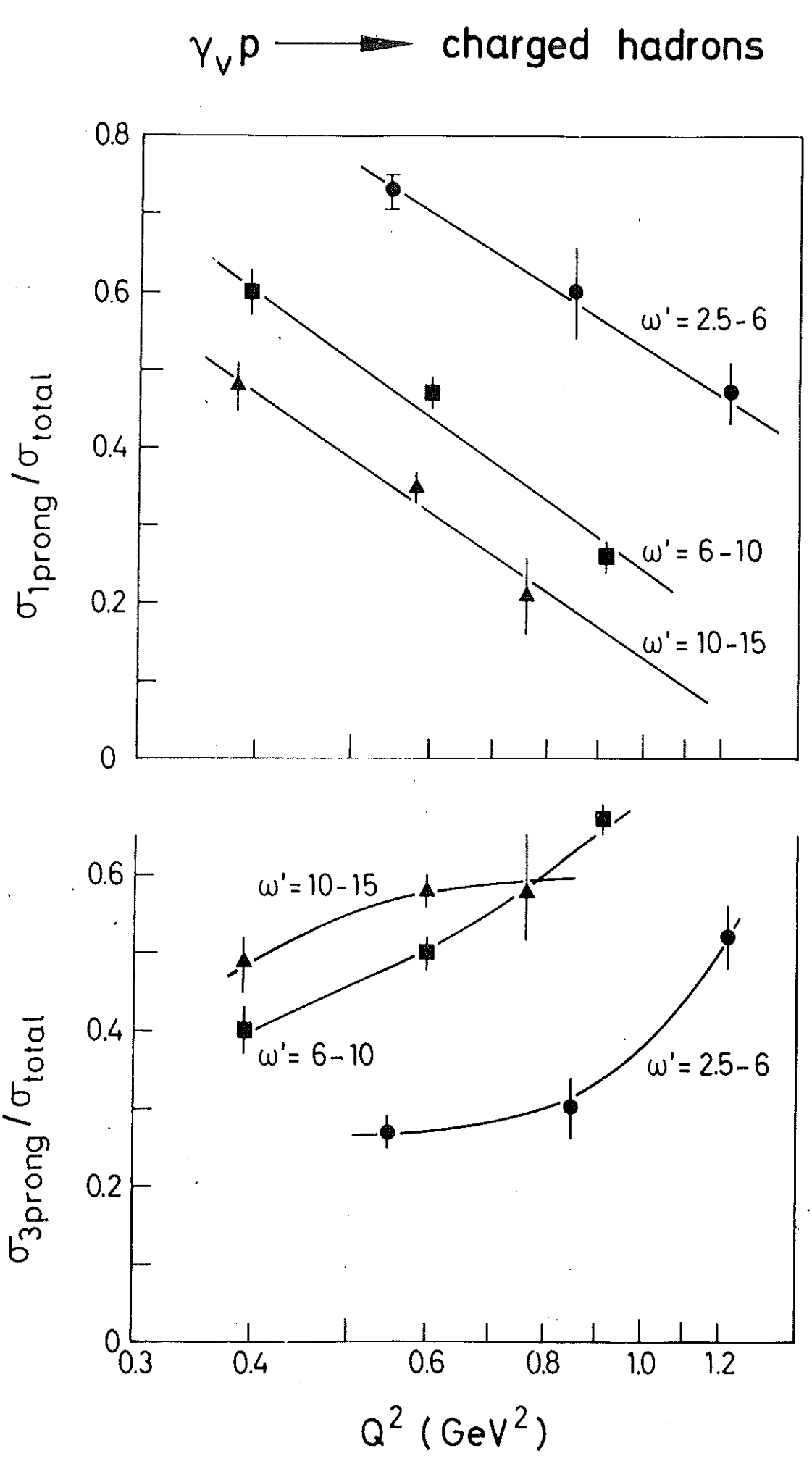
$\gamma_v p \longrightarrow$ charged hadrons
$\sigma_{1prong}/\sigma_{total}$
$\omega' = 2.5-6$
$\omega' = 6-10$
$\omega' = 10-15$
$\sigma_{3prong}/\sigma_{total}$
$\omega' = 10-15$
$\omega' = 6-10$
$\omega' = 2.5-6$
Q^2 (GeV^2)

Fig.5

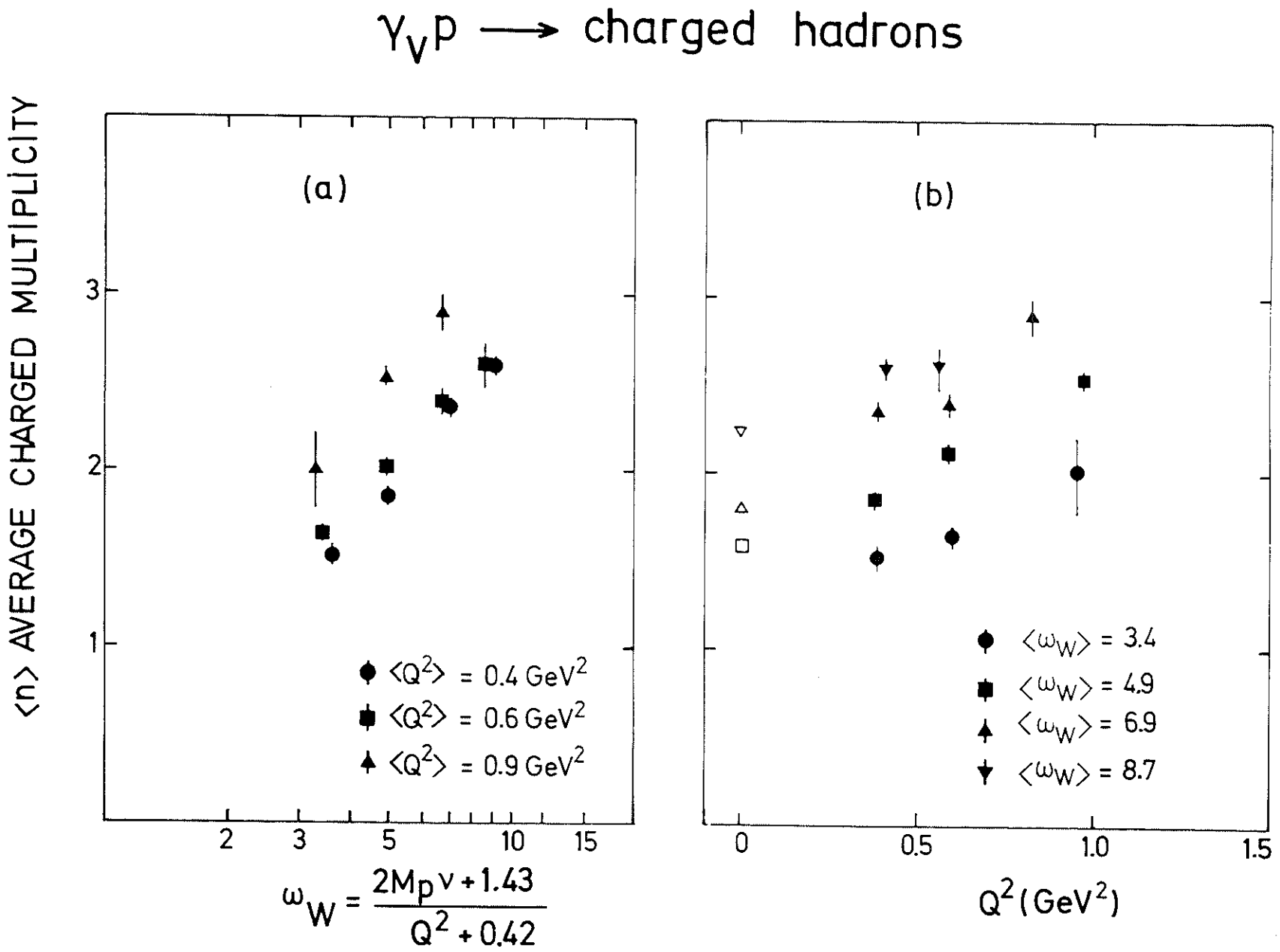
$\gamma_V p \longrightarrow$ charged hadrons
<n> AVERAGE CHARGED MULTIPLICITY
(a)
(b)
$\langle Q^2 \rangle$ = 0.4 GeV^2
$\langle Q^2 \rangle$ = 0.6 GeV^2
$\langle Q^2 \rangle$ = 0.9 GeV^2
$\langle \omega_W \rangle$ = 3.4
$\langle \omega_W \rangle$ = 4.9
$\langle \omega_W \rangle$ = 6.9
$\langle \omega_W \rangle$ = 8.7
$\omega_W = \frac{2Mp\nu + 1.43}{Q^2 + 0.42}$
Q^2 (GeV^2)

Fig.6

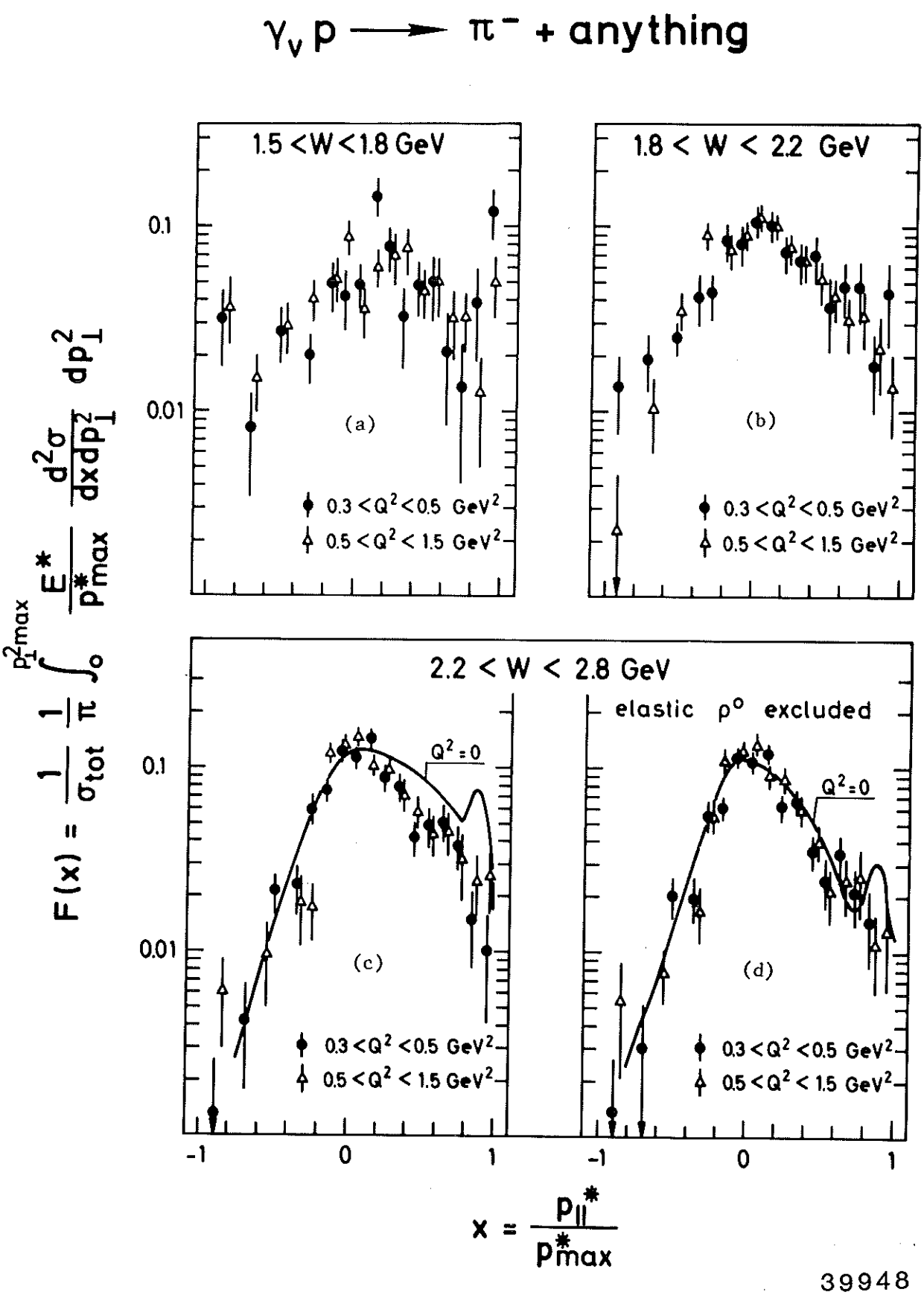
$\gamma_v p \longrightarrow \pi^- + \text{anything}$
1.5 < W < 1.8 GeV
1.8 < W < 2.2 GeV
2.2 < W < 2.8 GeV
elastic ρ^o excluded
$Q^2 = 0$
$0.3 < Q^2 < 0.5$ GeV^2
$0.5 < Q^2 < 1.5$ GeV^2
(a)
(b)
(c)
(d)
0.1
0.01
-1
0
1
$F(x) = \frac{1}{\sigma_{tot}} \frac{1}{\pi} \int_0^{p_\perp^{2max}} \frac{E^*}{p^*_{max}} \frac{d^2\sigma}{dx dp_\perp^2} dp_\perp^2$
$x = \frac{p_\parallel^*}{p^*_{max}}$
39948

Fig.7

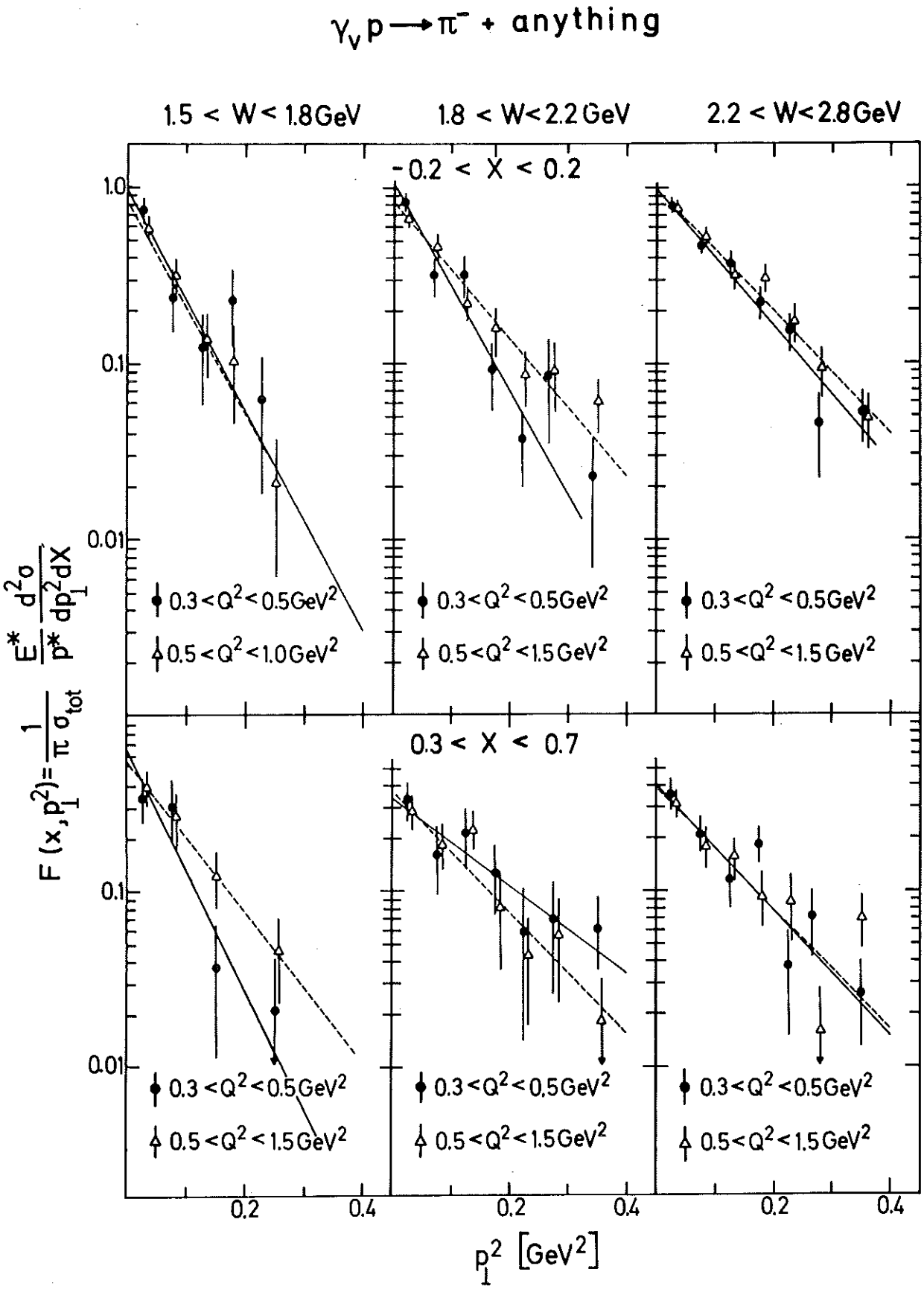
$\gamma_v p \longrightarrow \pi^- +$ anything
1.5 < W < 1.8GeV
1.8 < W < 2.2 GeV
2.2 < W < 2.8GeV
-0.2 < X < 0.2
0.3 < X < 0.7
$F(x,p_1^2) = \frac{1}{\pi}\frac{E^*}{p^*}\frac{d^2\sigma}{dp_1^2 dX}$
$\frac{1}{\pi\,\sigma_{tot}}$
0.3 < Q² < 0.5GeV²
0.5 < Q² < 1.0GeV²
0.5 < Q² < 1.5GeV²
1.0
0.1
0.01
0.2
0.4
p_1^2 [GeV²]

Fig.8

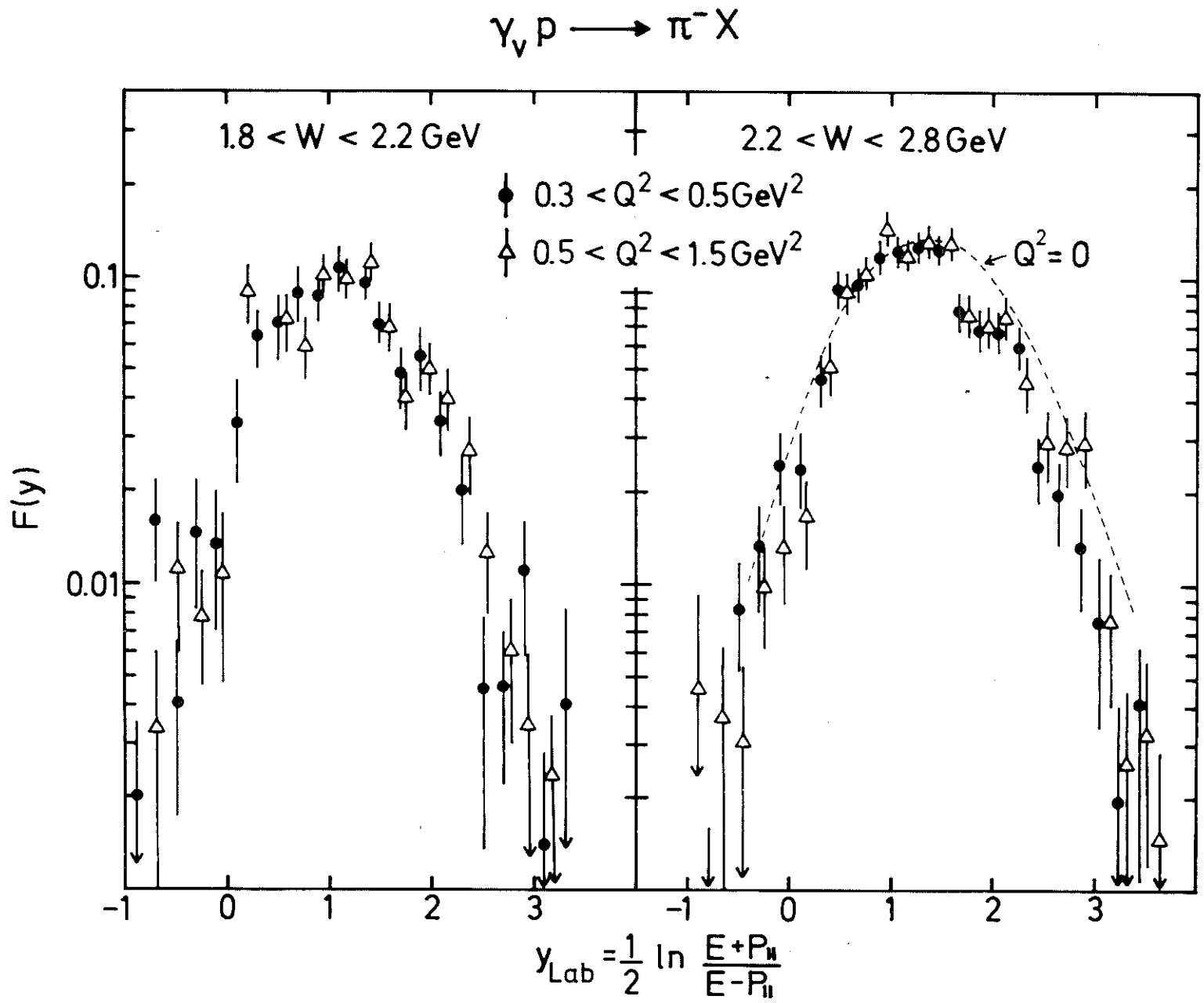
$\gamma_v p \longrightarrow \pi^- X$
1.8 < W < 2.2 GeV
2.2 < W < 2.8 GeV
0.3 < Q² < 0.5 GeV²
0.5 < Q² < 1.5 GeV²
Q² = 0
F(y)
0.1
0.01
-1
0
1
2
3
$y_{Lab} = \frac{1}{2} \ln \frac{E+P_{\parallel}}{E-P_{\parallel}}$

Fig.9

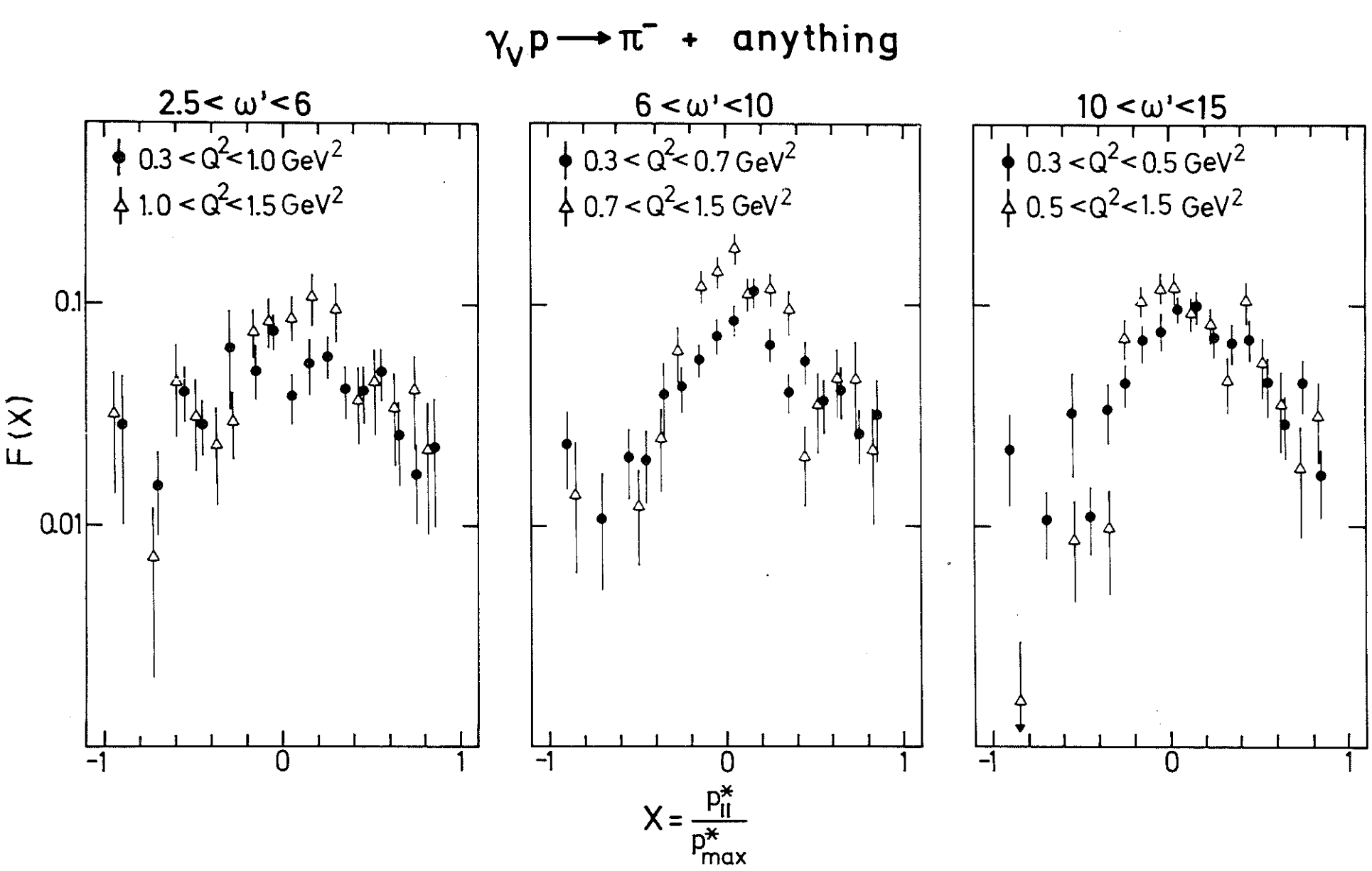
$\gamma_V p \longrightarrow \pi^- +$ anything
2.5< ω'<6
6 <ω'<10
10 <ω'<15
0.3 < Q²< 1.0 GeV²
1.0 < Q²< 1.5 GeV²
0.3 < Q²< 0.7 GeV²
0.7 < Q²< 1.5 GeV²
0.3 < Q²< 0.5 GeV²
0.5 < Q²< 1.5 GeV²
F(X)
0.1
0.01
-1
0
1
$X = \frac{p^*_{II}}{p^*_{max}}$

Fig. 10

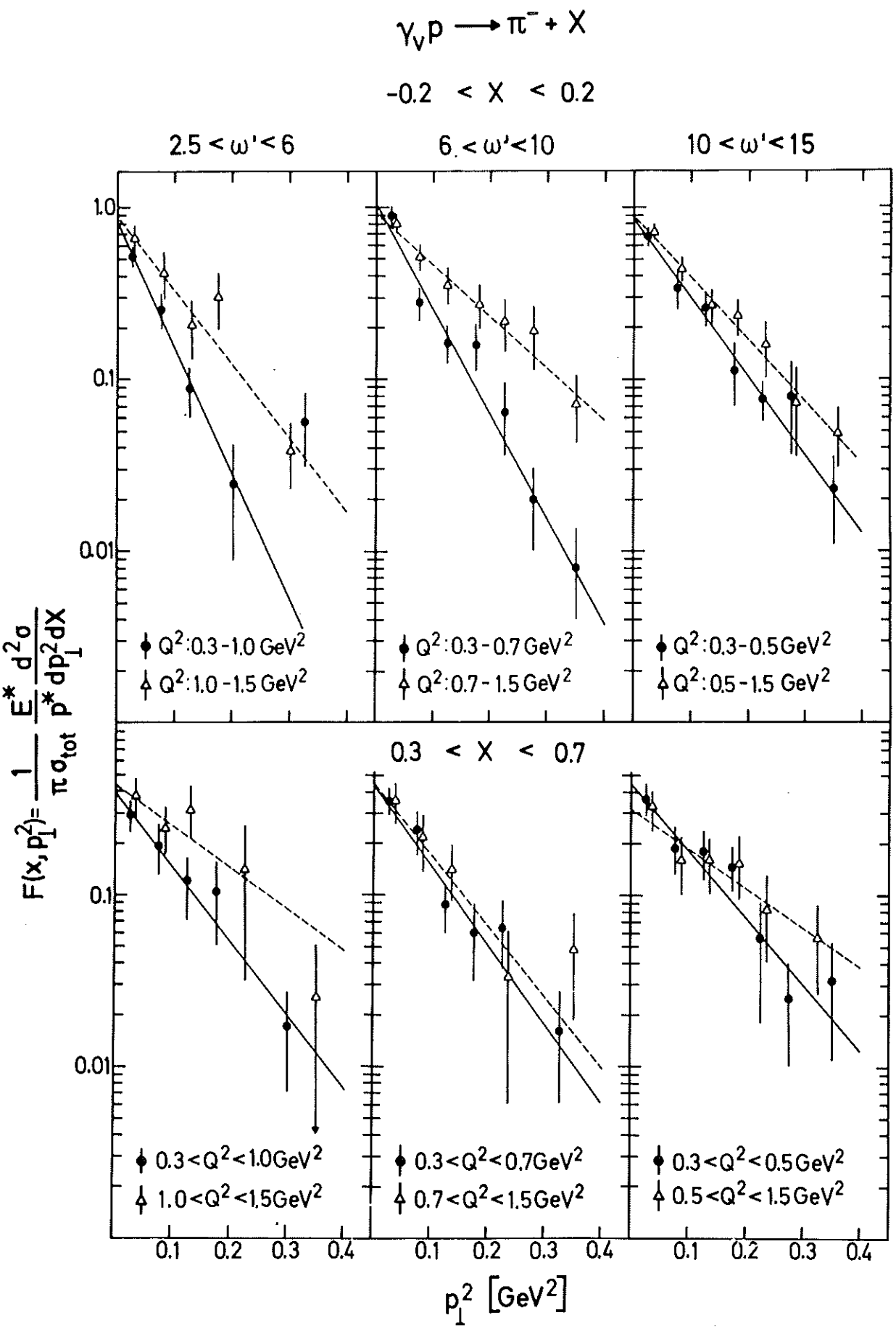
$\gamma_v p \longrightarrow \pi^- + X$
$-0.2 < X < 0.2$
$2.5 < \omega' < 6$
$6 < \omega' < 10$
$10 < \omega' < 15$
Q^2:0.3-1.0 GeV^2
Q^2:1.0-1.5 GeV^2
Q^2:0.3-0.7 GeV^2
Q^2:0.7-1.5 GeV^2
Q^2:0.3-0.5 GeV^2
Q^2:0.5-1.5 GeV^2
$0.3 < X < 0.7$
$0.3<Q^2<1.0$ GeV^2
$1.0<Q^2<1.5$ GeV^2
$0.3<Q^2<0.7$ GeV^2
$0.7<Q^2<1.5$ GeV^2
$0.3<Q^2<0.5$ GeV^2
$0.5<Q^2<1.5$ GeV^2
$F(x,p_\perp^2)=\frac{1}{\pi\sigma_{tot}}\frac{E^*}{p^*}\frac{d^2\sigma}{dp_\perp^2 dX}$
$p_\perp^2$ [GeV^2]
1.0
0.1
0.01
0.1
0.2
0.3
0.4

Fig. 11

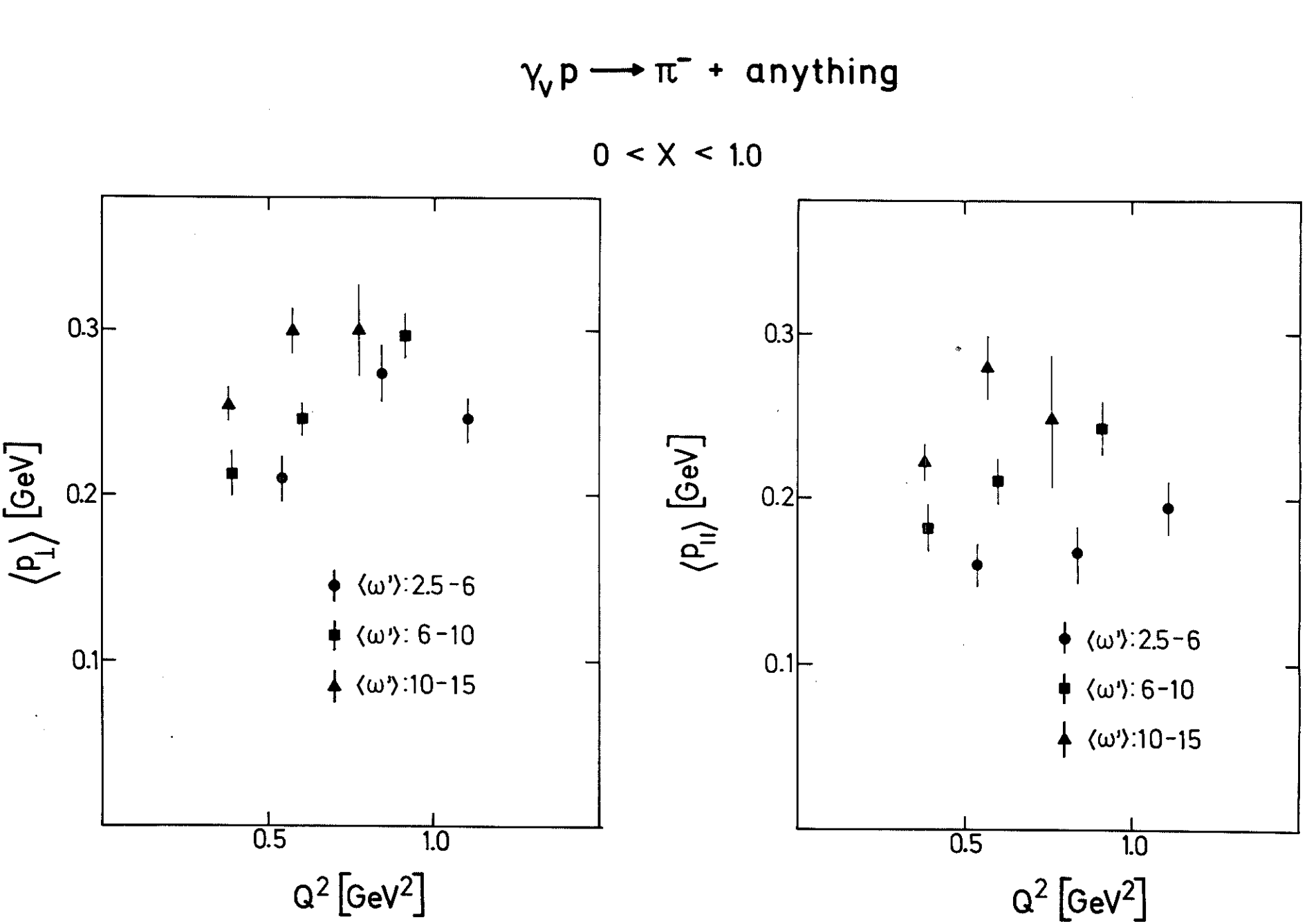
$\gamma_v p \longrightarrow \pi^- +$ anything
$0 < X < 1.0$
$\langle p_\perp \rangle$ [GeV]
$\langle p_{\parallel} \rangle$ [GeV]
0.3
0.2
0.1
0.5
1.0
Q^2 [GeV^2]
$\langle \omega' \rangle$: 2.5 - 6
$\langle \omega' \rangle$: 6 - 10
$\langle \omega' \rangle$: 10 - 15

Fig. 12

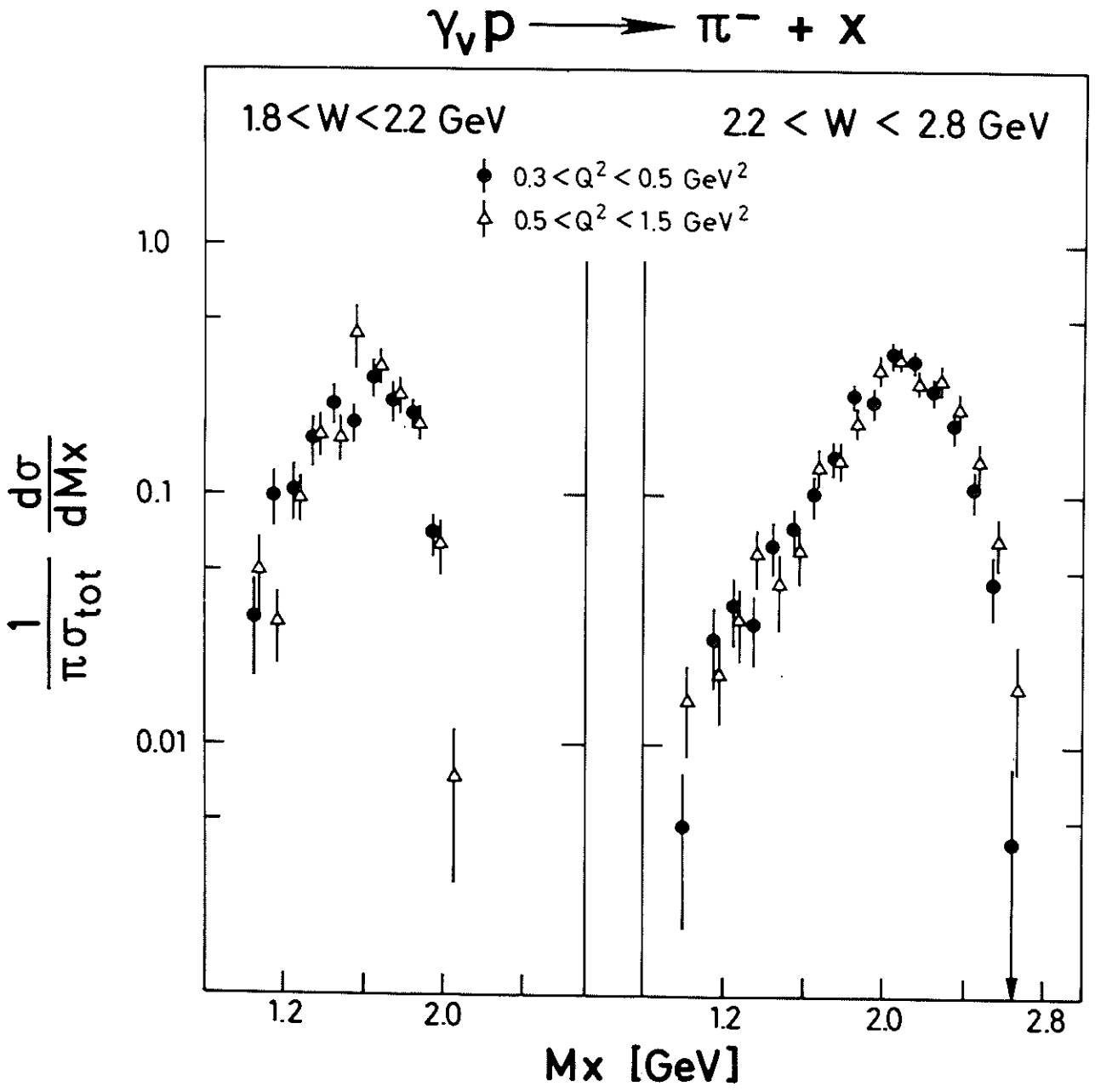
$\gamma_v p \longrightarrow \pi^- + X$
1.8 < W < 2.2 GeV
2.2 < W < 2.8 GeV
$0.3 < Q^2 < 0.5$ GeV^2
$0.5 < Q^2 < 1.5$ GeV^2
$\frac{1}{\pi\sigma_{tot}} \frac{d\sigma}{dMx}$
1.0
0.1
0.01
1.2
2.0
1.2
2.0
2.8
Mx [GeV]

Fig. 13

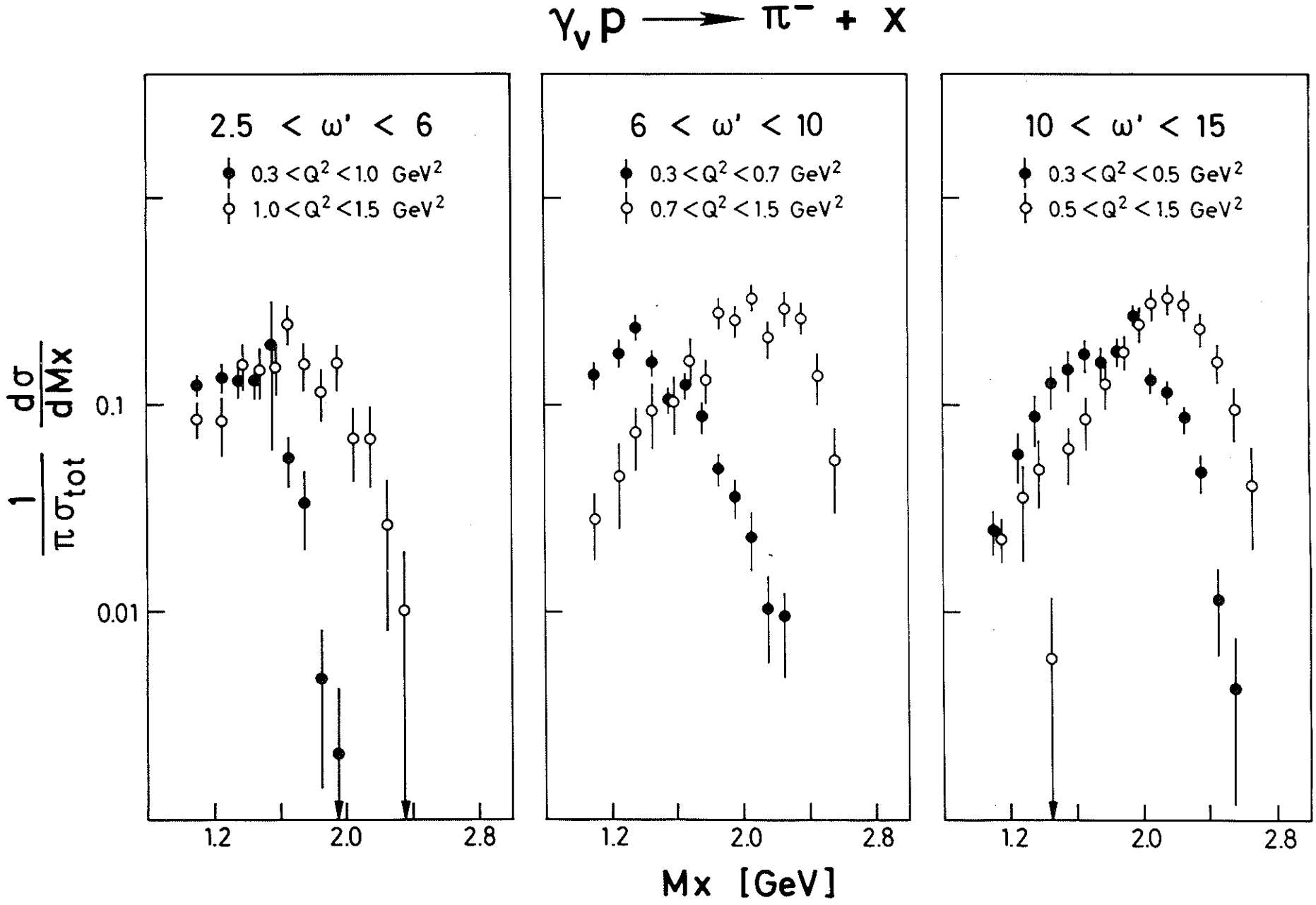
$\gamma_v p \longrightarrow \pi^- + X$
2.5 < ω' < 6
0.3 < Q² < 1.0 GeV²
1.0 < Q² < 1.5 GeV²
6 < ω' < 10
0.3 < Q² < 0.7 GeV²
0.7 < Q² < 1.5 GeV²
10 < ω' < 15
0.3 < Q² < 0.5 GeV²
0.5 < Q² < 1.5 GeV²
$\frac{1}{\pi\sigma_{tot}} \frac{d\sigma}{dMx}$
0.1
0.01
1.2
2.0
2.8
Mx [GeV]

Fig. 14

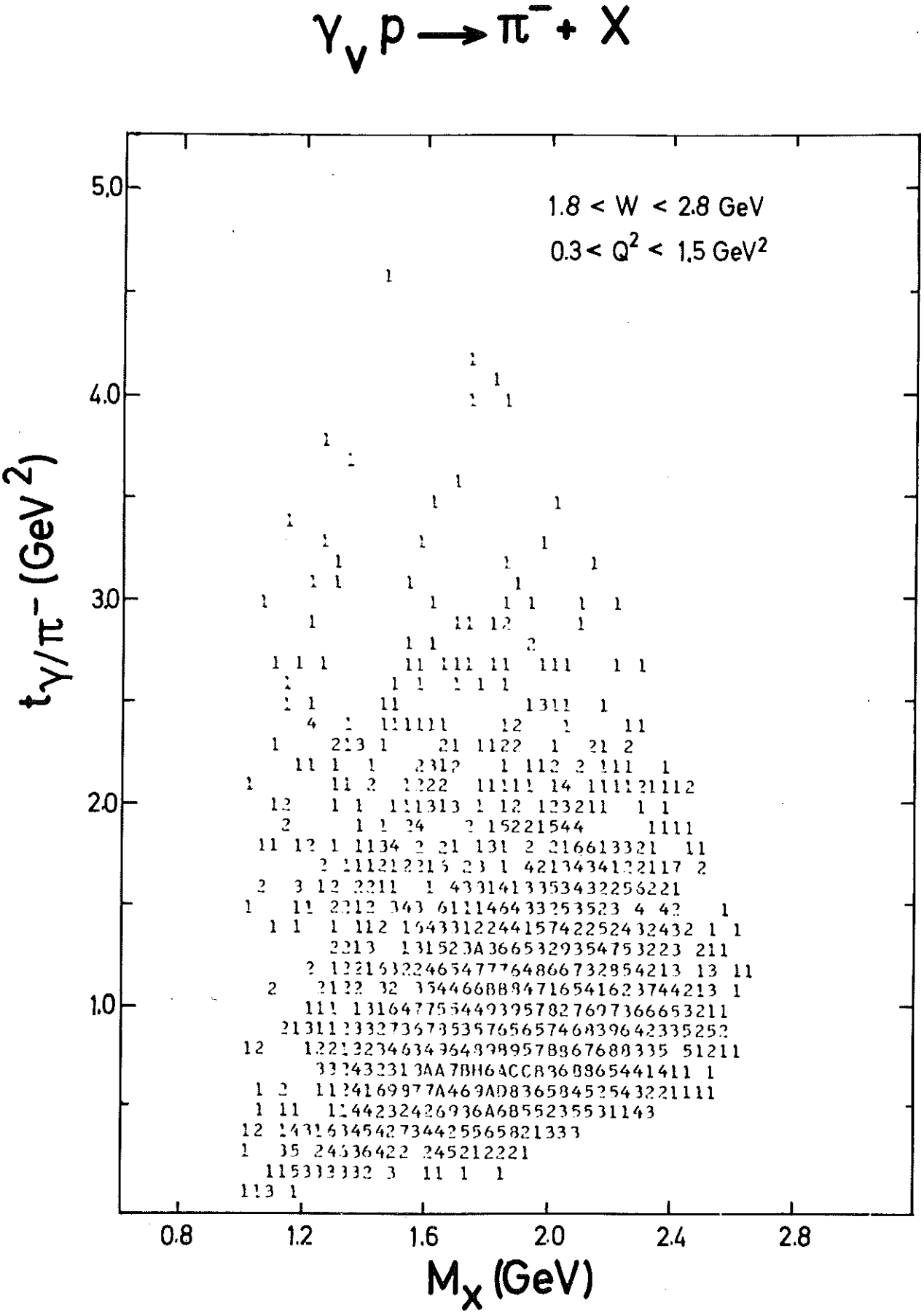
$\gamma_v p \longrightarrow \pi^- + X$
1.8 < W < 2.8 GeV
0.3 < Q² < 1.5 GeV²
t_{γ/π^-} (GeV²)
5.0
4.0
3.0
2.0
1.0
0.8
1.2
1.6
2.0
2.4
2.8
M_X (GeV)

Fig. 15

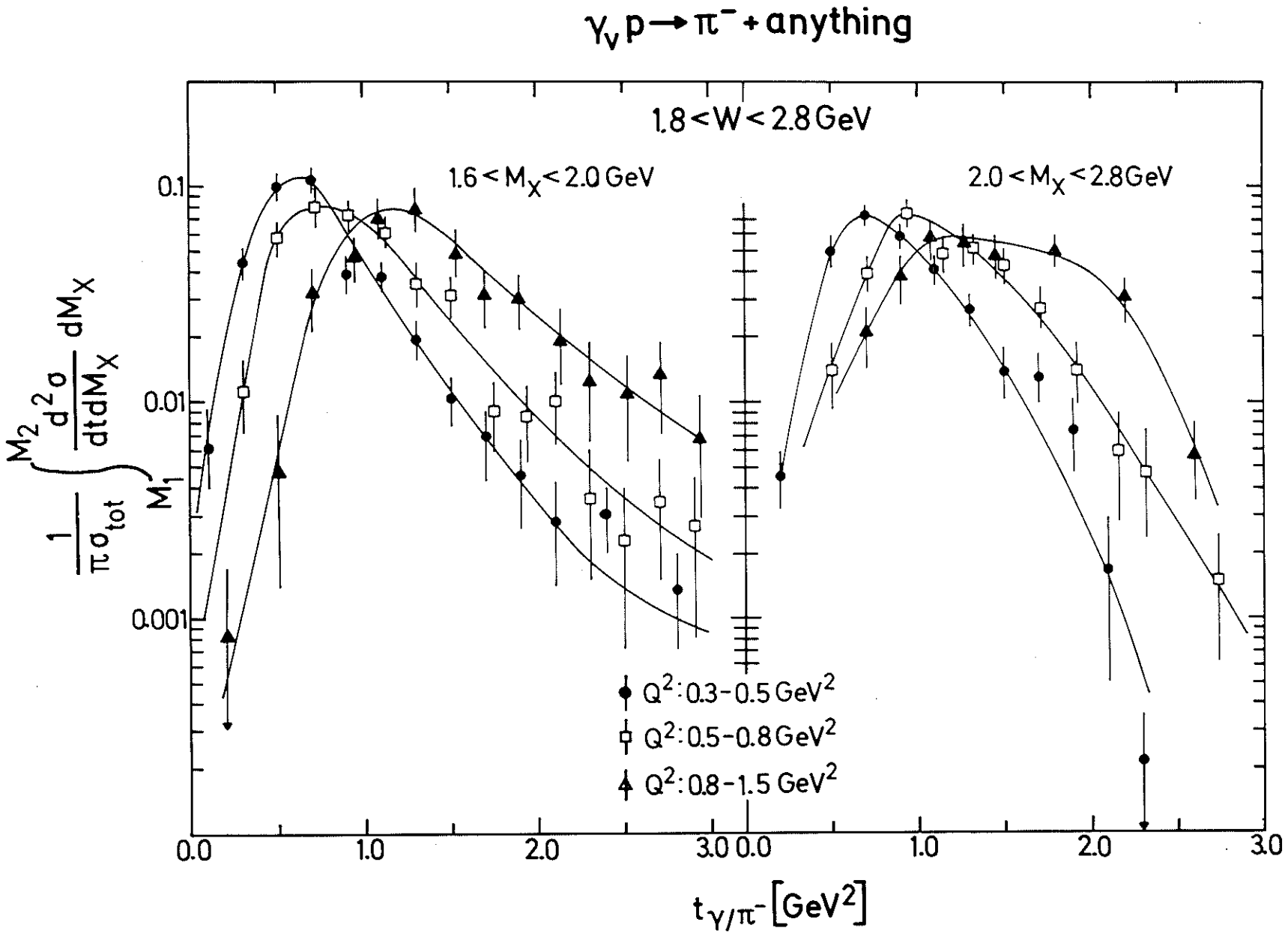
$\gamma_v p \rightarrow \pi^- +$ anything
1.8 < W < 2.8 GeV
1.6 < M_X < 2.0 GeV
2.0 < M_X < 2.8 GeV
$\frac{1}{\pi \sigma_{tot}} \int_{M_1}^{M_2} \frac{d^2\sigma}{dt dM_X} dM_X$
0.1
0.01
0.001
Q^2: 0.3 - 0.5 GeV^2
Q^2: 0.5 - 0.8 GeV^2
Q^2: 0.8 - 1.5 GeV^2
0.0
1.0
2.0
3.0
t_{γ/π^-} [GeV^2]

Fig. 16

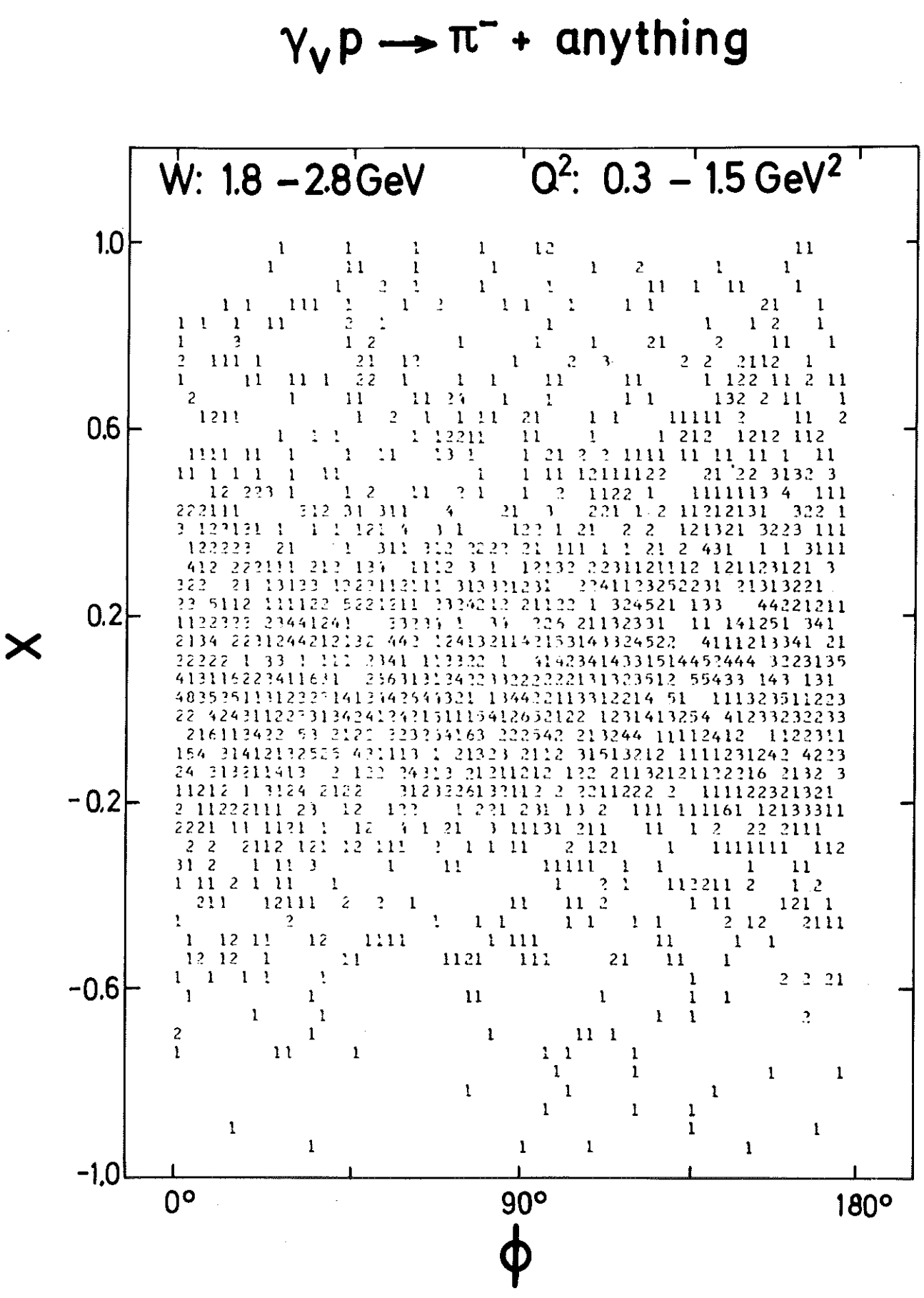
$\gamma_V p \rightarrow \pi^- +$ anything
W: 1.8 – 2.8 GeV
Q^2: 0.3 – 1.5 GeV^2
1.0
0.6
0.2
-0.2
-0.6
-1.0
X
0°
90°
180°
Φ

Fig.17

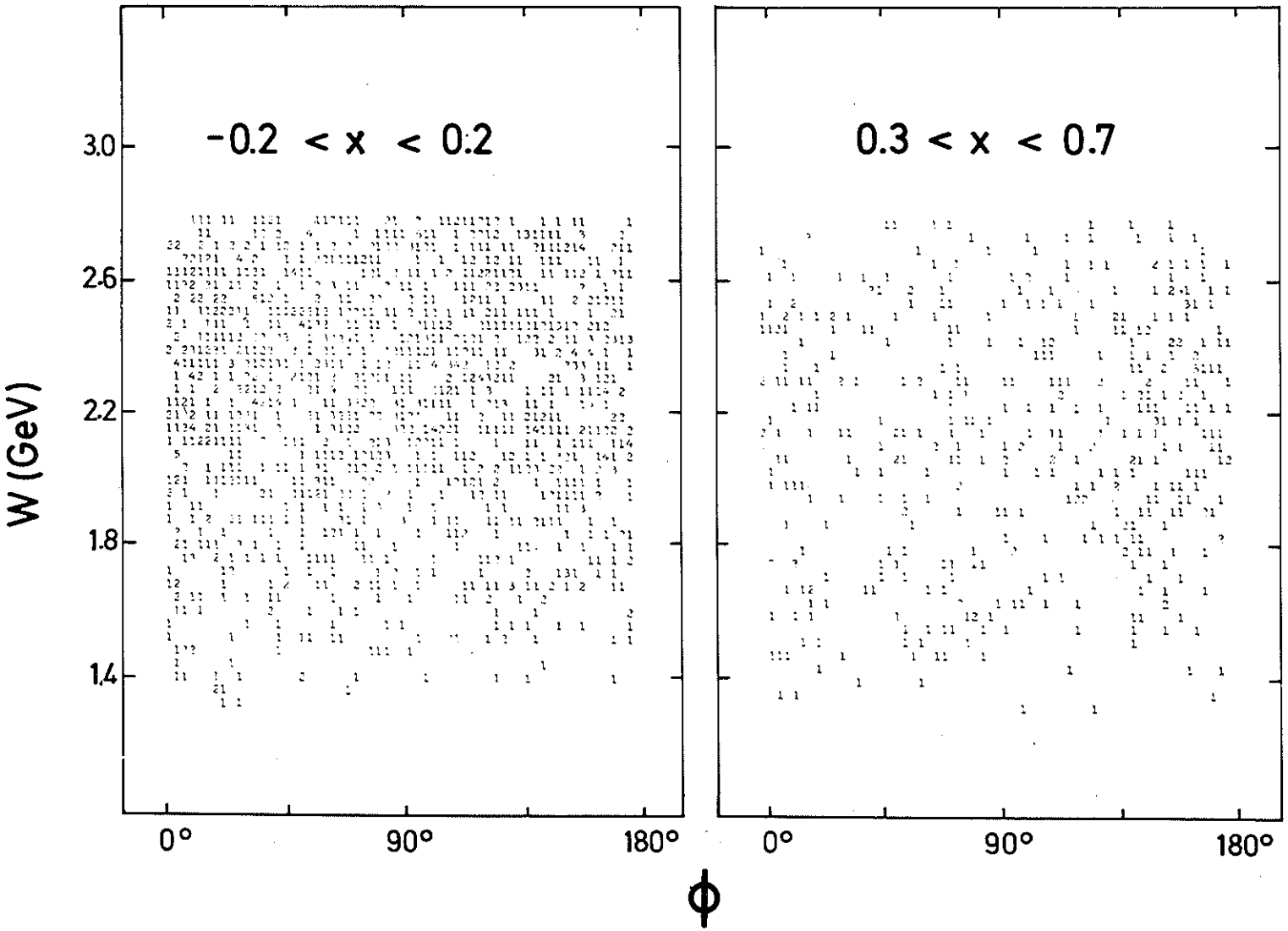
$\gamma_v p \longrightarrow \pi^- +$ anything
$0.3 < Q^2 < 1.5$ GeV^2
$-0.2 < x < 0.2$
$0.3 < x < 0.7$
W (GeV)
3.0
2.6
2.2
1.8
1.4
0°
90°
180°
0°
90°
180°
ϕ

Fig.18

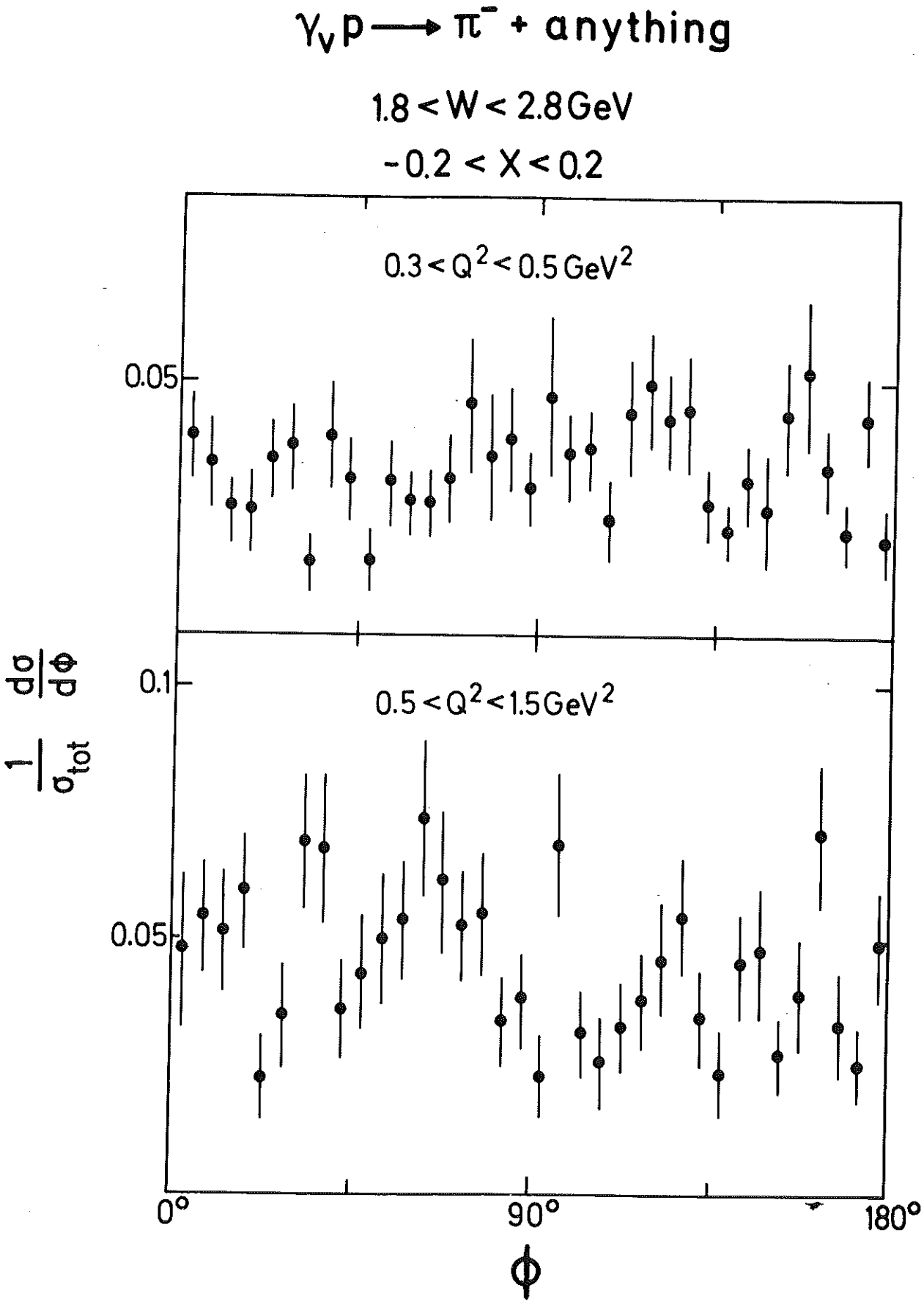
$\gamma_v p \longrightarrow \pi^- +$ anything
$1.8 < W < 2.8\,GeV$
$-0.2 < X < 0.2$
$0.3 < Q^2 < 0.5\,GeV^2$
$0.5 < Q^2 < 1.5\,GeV^2$
0.05
0.1
0.05
$\frac{1}{\sigma_{tot}} \frac{d\sigma}{d\phi}$
0°
90°
180°
ϕ

Fig. 19

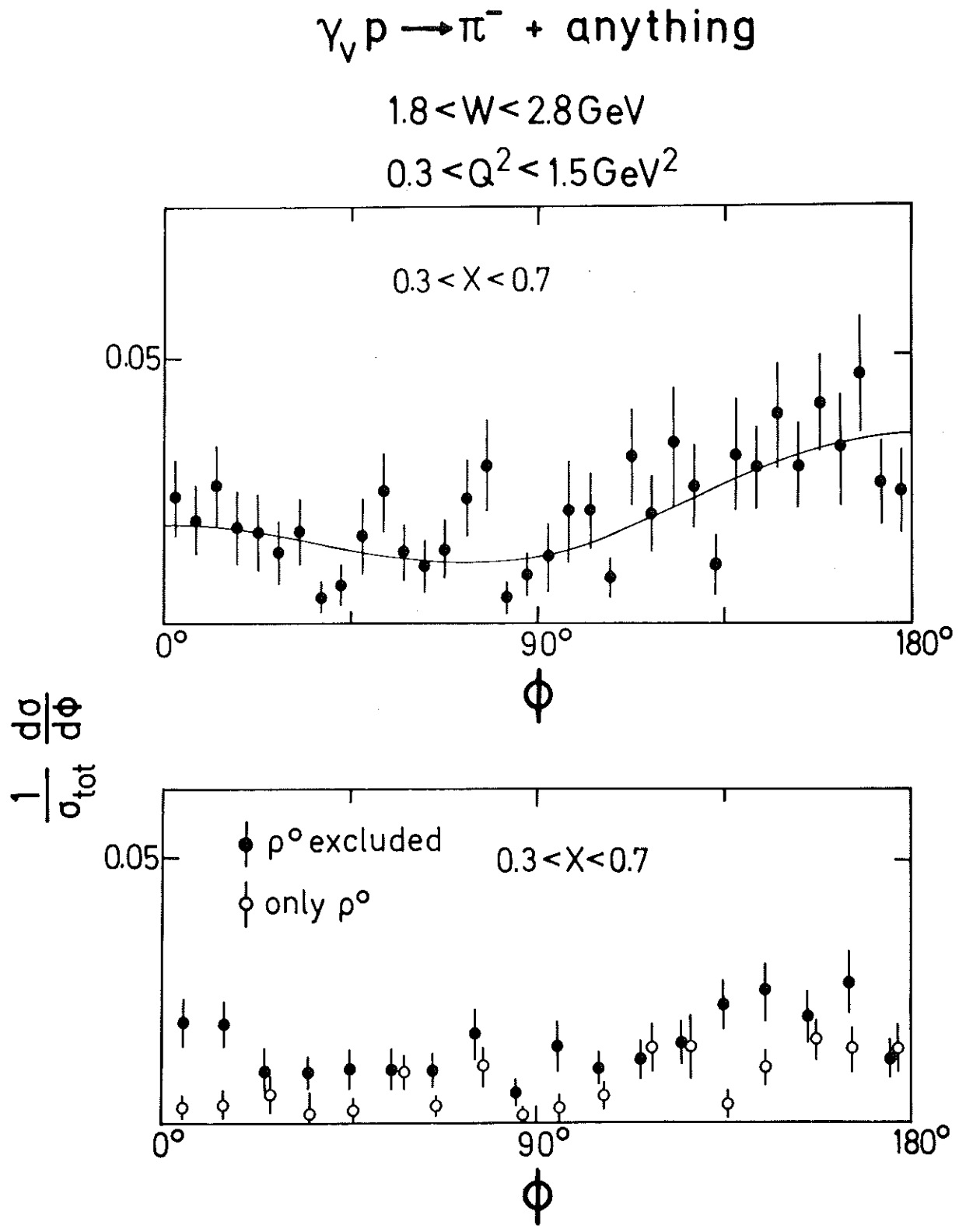
$\gamma_v p \longrightarrow \pi^- +$ anything
$1.8 < W < 2.8\,GeV$
$0.3 < Q^2 < 1.5\,GeV^2$
$0.3 < X < 0.7$
0.05
0°
90°
180°
Φ
$\frac{1}{\sigma_{tot}} \frac{d\sigma}{d\Phi}$
ρ° excluded
only ρ°
$0.3 < X < 0.7$
0.05
0°
90°
180°
Φ

Fig.20

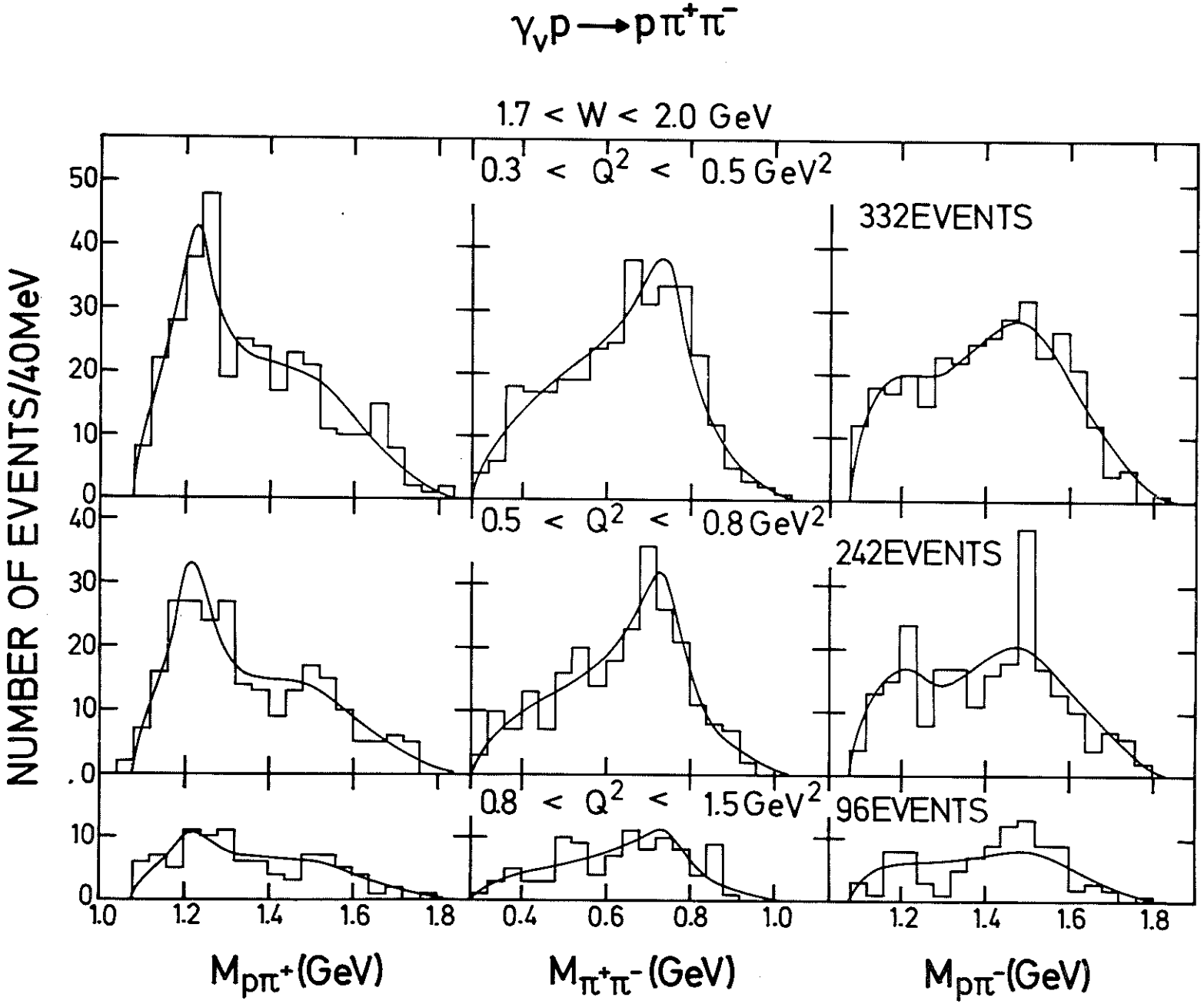
$\gamma_v p \longrightarrow p\pi^+\pi^-$
1.7 < W < 2.0 GeV
0.3 < Q² < 0.5 GeV²
332EVENTS
0.5 < Q² < 0.8 GeV²
242EVENTS
0.8 < Q² < 1.5 GeV²
96EVENTS
NUMBER OF EVENTS/40MeV
$M_{p\pi^+}$(GeV)
$M_{\pi^+\pi^-}$(GeV)
$M_{p\pi^-}$(GeV)

Fig.21

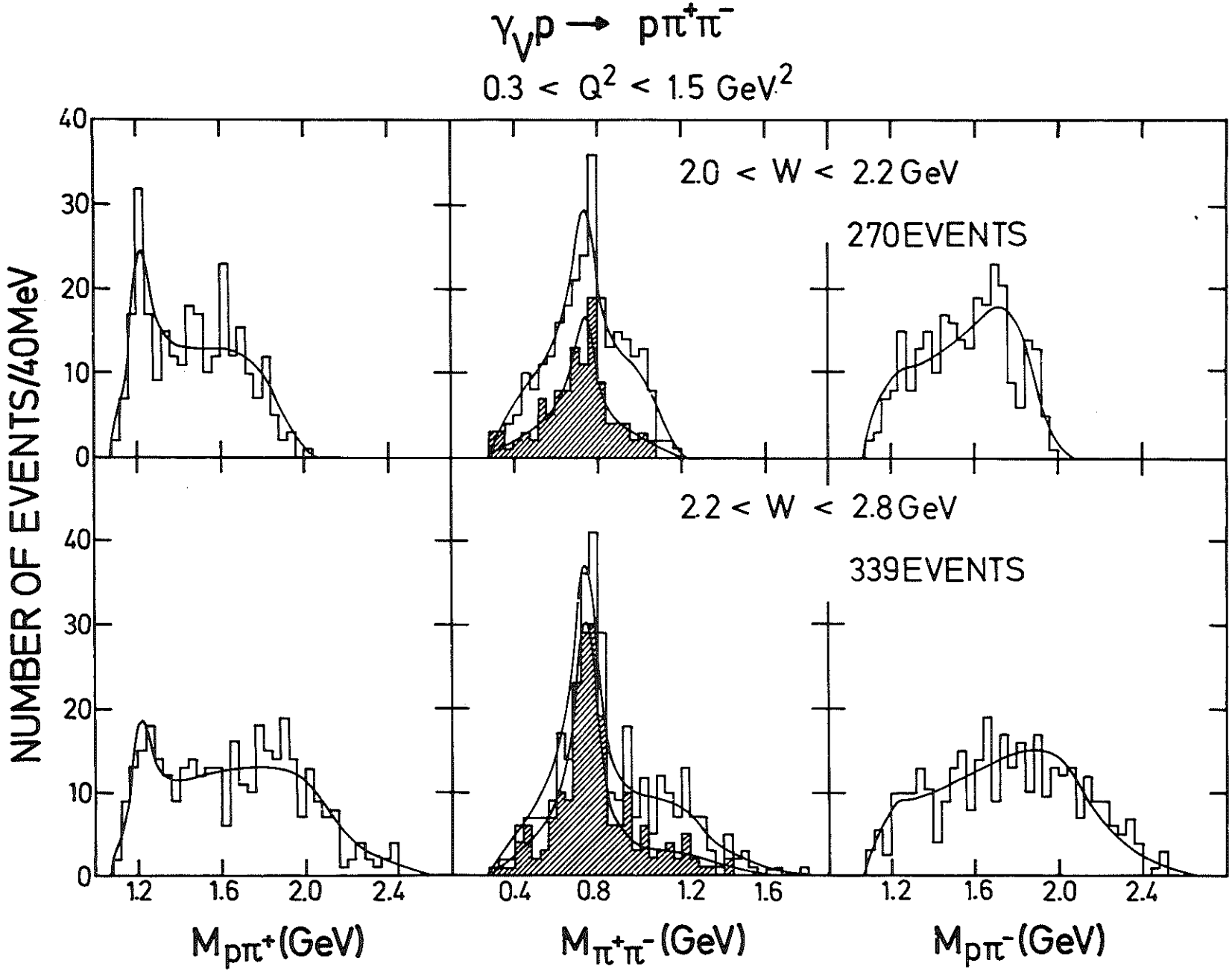
$\gamma_V p \rightarrow p\pi^+\pi^-$
$0.3 < Q^2 < 1.5\ GeV^2$
$2.0 < W < 2.2\,GeV$
270EVENTS
$2.2 < W < 2.8\,GeV$
339EVENTS
NUMBER OF EVENTS/40MeV
$M_{p\pi^+}(GeV)$
$M_{\pi^+\pi^-}(GeV)$
$M_{p\pi^-}(GeV)$

Fig.22

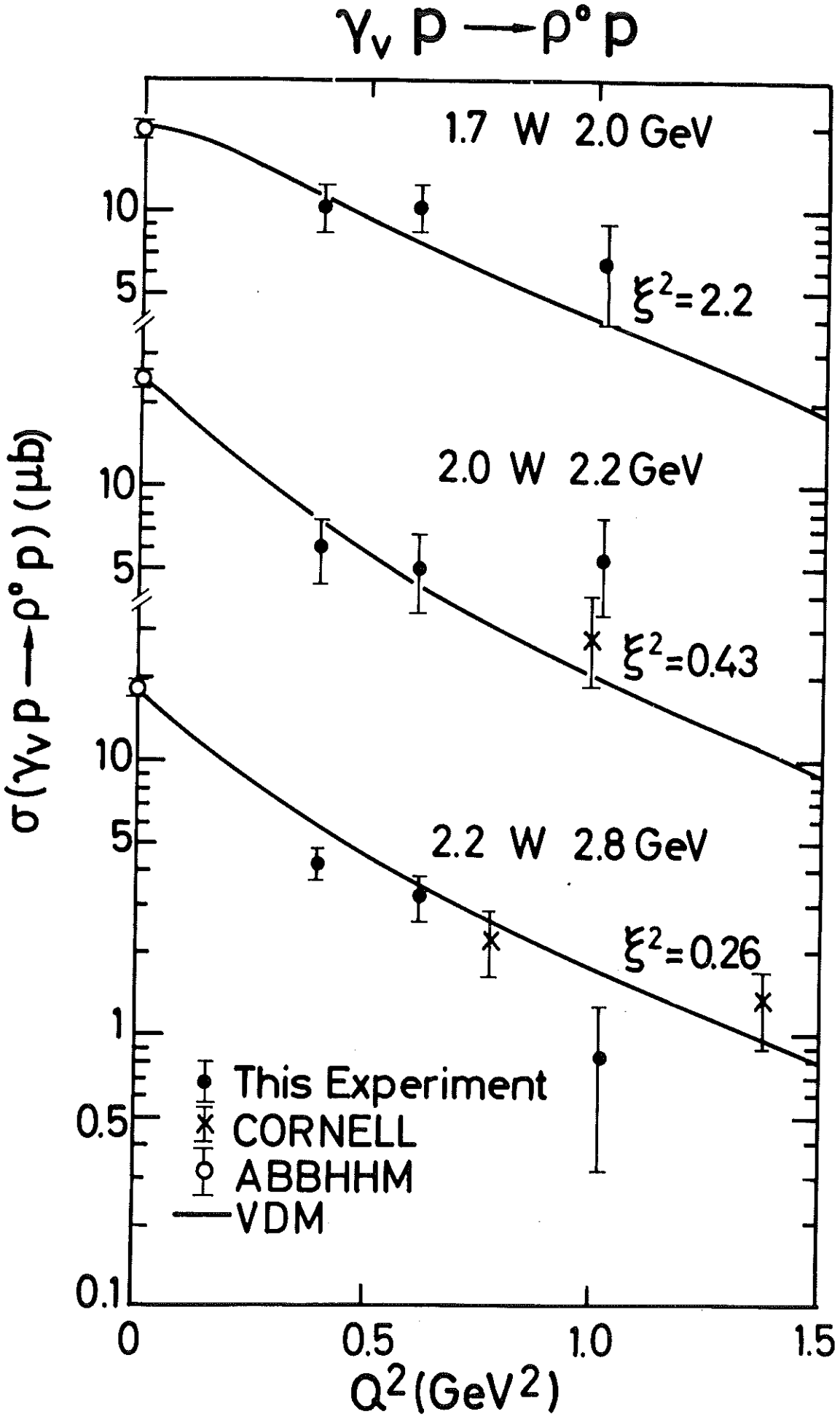
$\gamma_v p \rightarrow \rho^0 p$
1.7 W 2.0 GeV
$\xi^2=2.2$
2.0 W 2.2 GeV
$\xi^2=0.43$
2.2 W 2.8 GeV
$\xi^2=0.26$
This Experiment
CORNELL
ABBHHM
VDM
$\sigma(\gamma_v p \rightarrow \rho^0 p)$ (μb)
Q^2 (GeV^2)
10
5
1
0.5
0.1
0
0.5
1.0
1.5

Fig.23

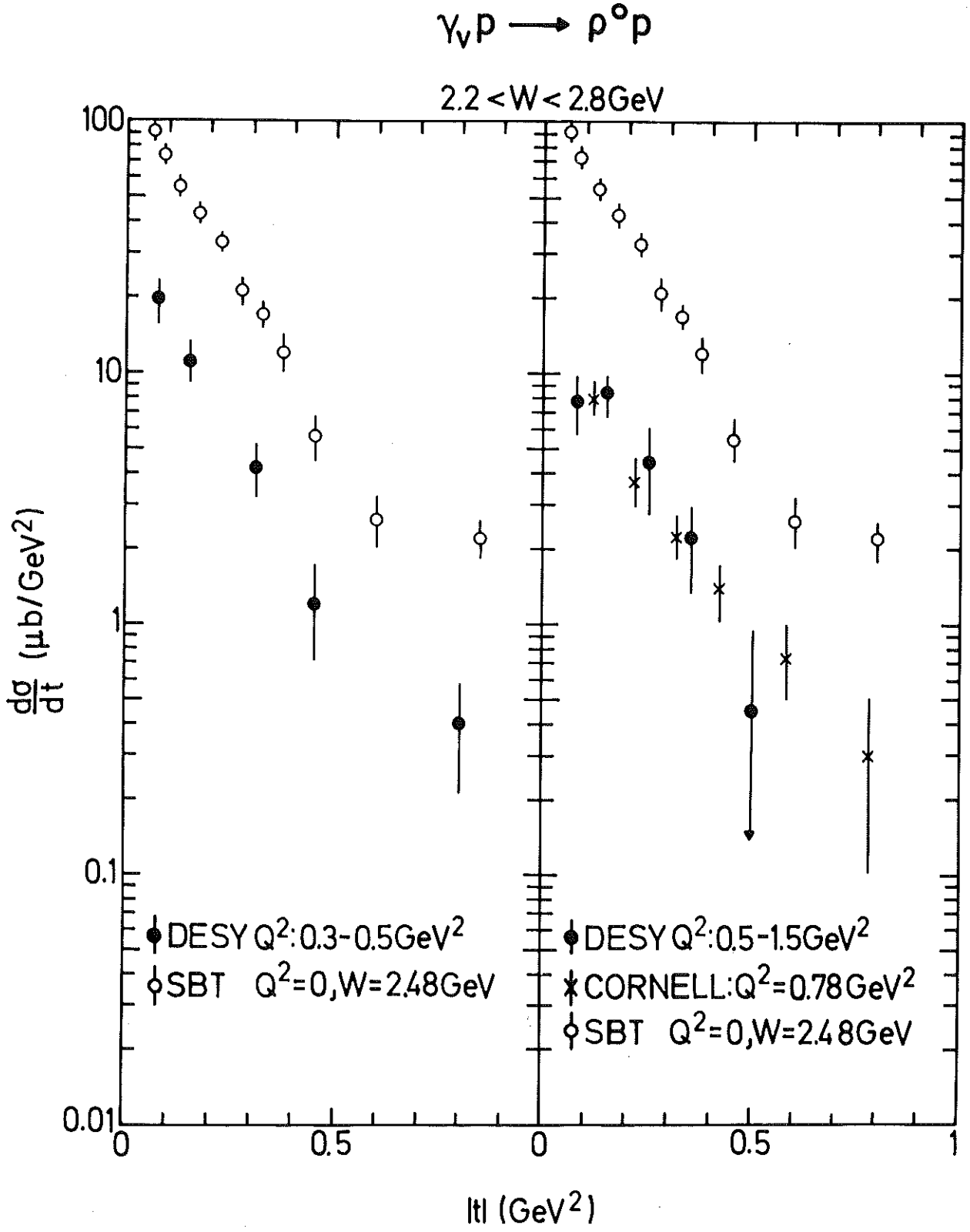
$\gamma_v p \longrightarrow \rho^o p$
2.2 < W < 2.8GeV
100
10
1
0.1
0.01
$\frac{d\sigma}{dt}$ (μb/GeV²)
DESY Q²:0.3-0.5GeV²
SBT Q²=0,W=2.48GeV
DESY Q²:0.5-1.5GeV²
CORNELL:Q²=0.78GeV²
SBT Q²=0,W=2.48GeV
0
0.5
0
0.5
1
|t| (GeV²)

Fig.24

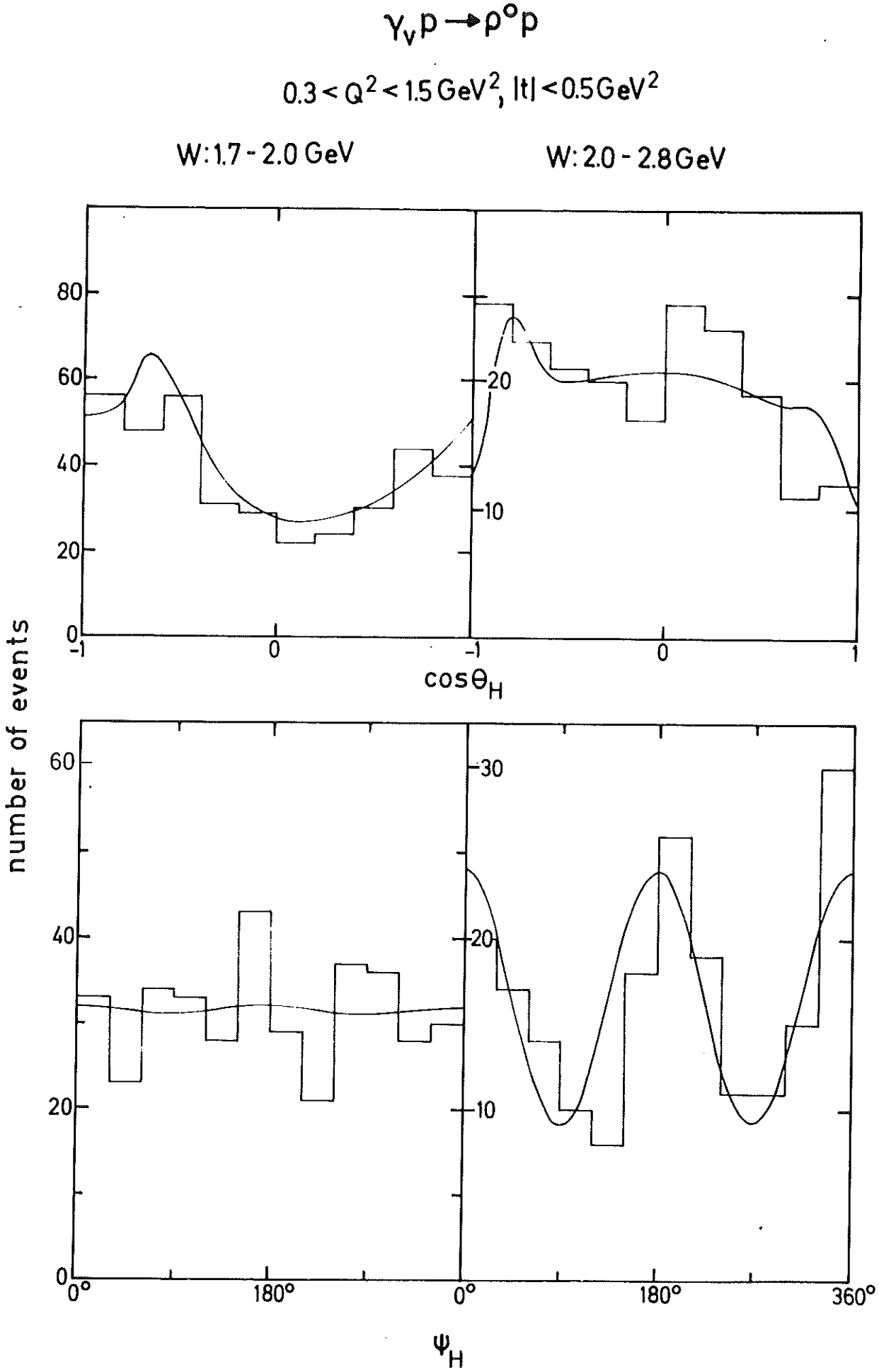
$\gamma_v p \rightarrow \rho^0 p$
$0.3 < Q^2 < 1.5\,GeV^2$, $|t| < 0.5\,GeV^2$
W: 1.7 - 2.0 GeV
W: 2.0 - 2.8 GeV
number of events
$\cos\Theta_H$
Ψ_H
0°
180°
360°

Fig.25

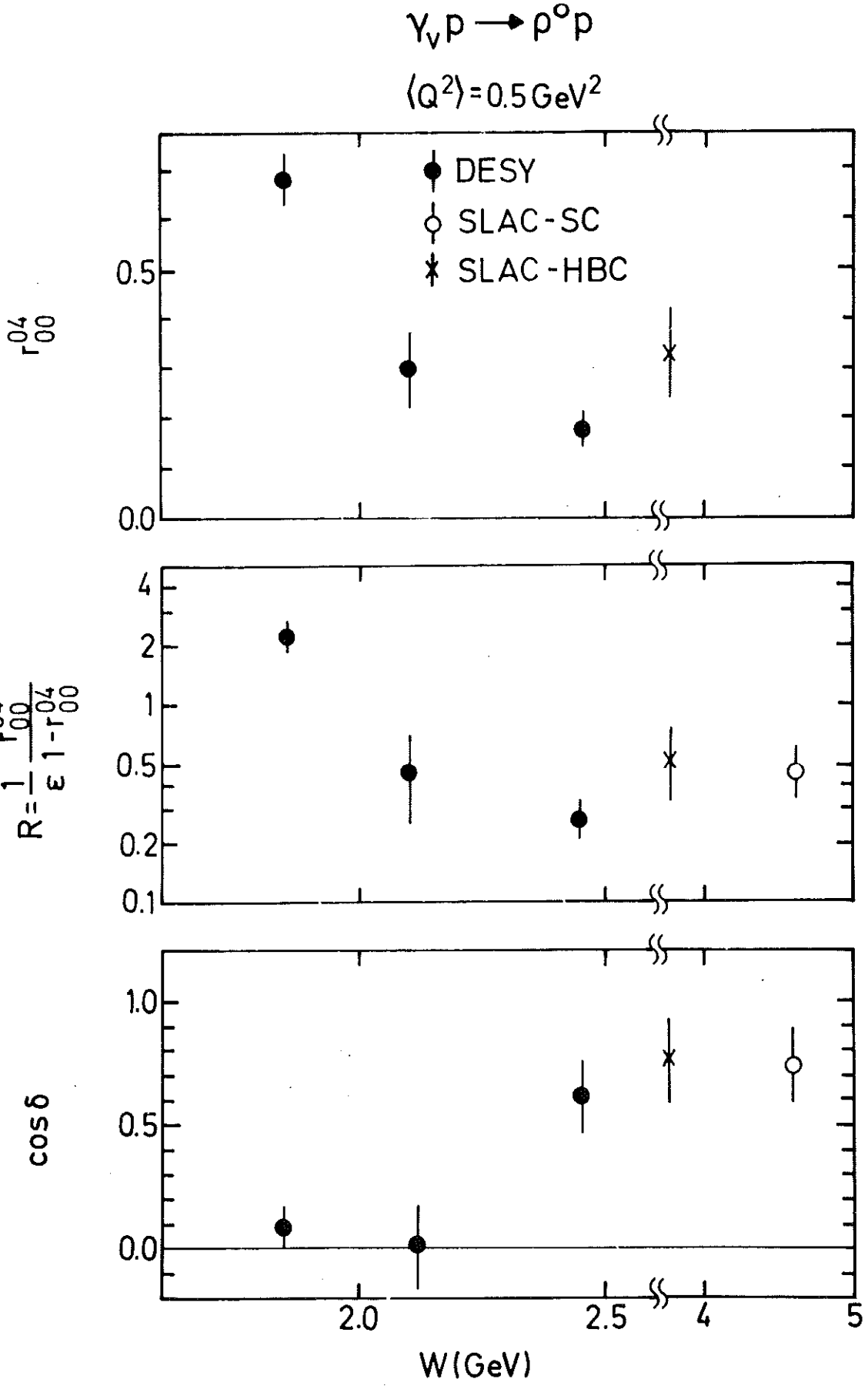
$\gamma_v p \rightarrow \rho^o p$
$\langle Q^2 \rangle = 0.5\,GeV^2$
DESY
SLAC-SC
SLAC-HBC
r_{00}^{04}
$R = \frac{1}{\varepsilon}\frac{r_{00}^{04}}{1-r_{00}^{04}}$
$\cos\delta$
0.0
0.5
0.1
0.2
1
2
4
1.0
2.0
2.5
5
W(GeV)

Fig.26

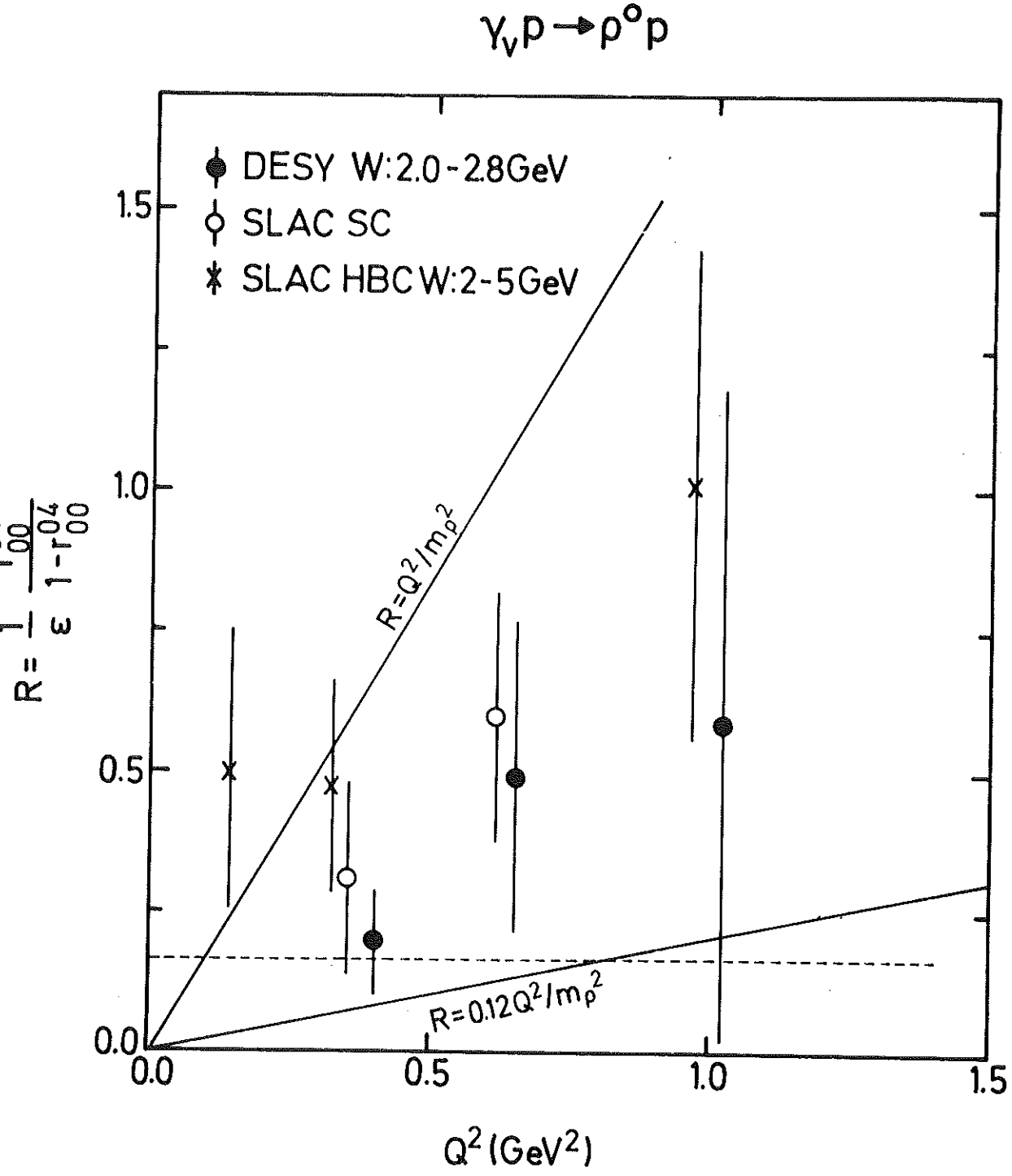
$\gamma_V p \rightarrow \rho^0 p$
DESY W:2.0-2.8GeV
SLAC SC
SLAC HBC W:2-5GeV
$R=Q^2/m_\rho^2$
$R=0.12Q^2/m_\rho^2$
$R=\frac{1}{\varepsilon}\frac{r_{00}^{04}}{1-r_{00}^{04}}$
Q^2 (GeV^2)
0.0
0.5
1.0
1.5

Fig.27

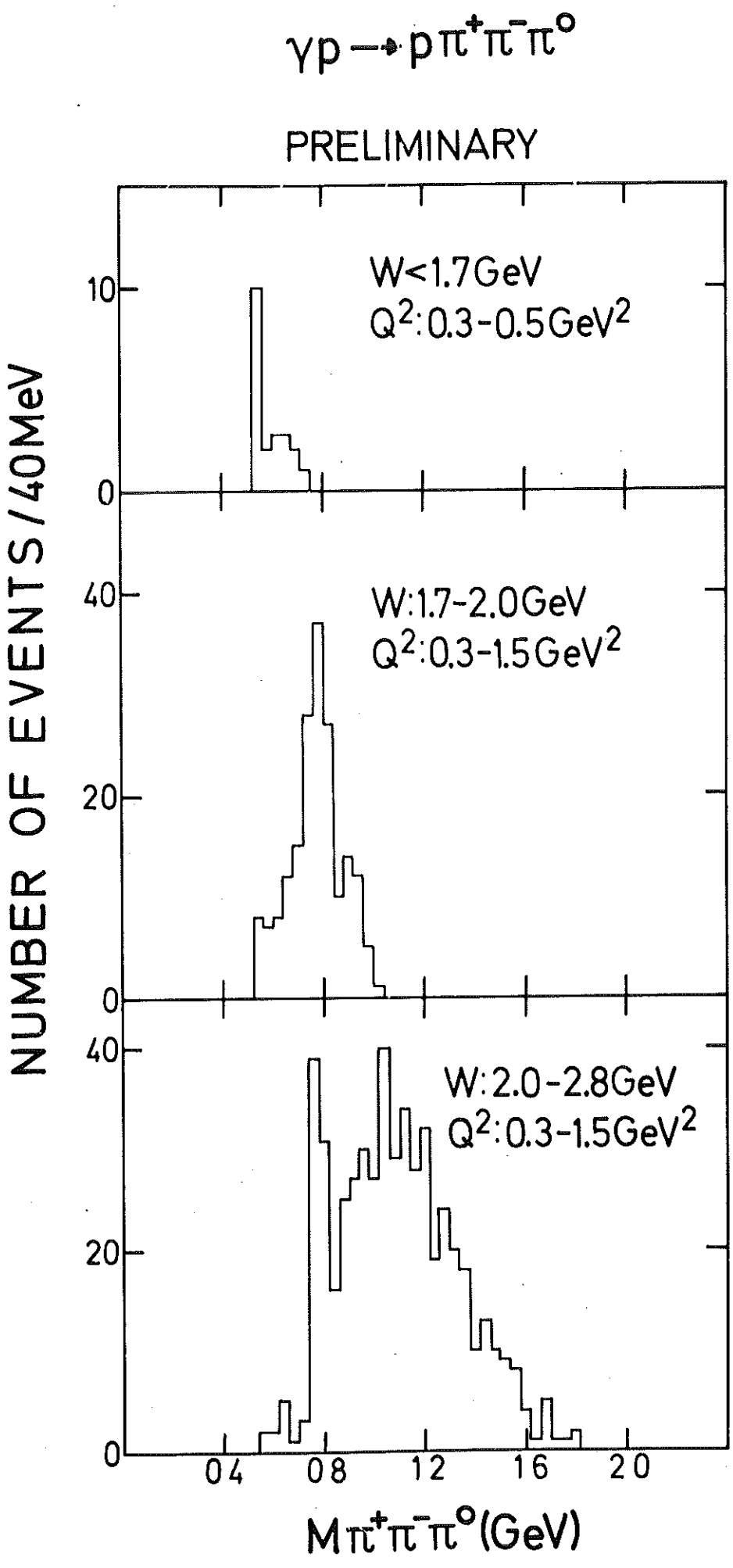
γp → pπ⁺π⁻π°
PRELIMINARY
W<1.7GeV
Q²:0.3-0.5GeV²
W:1.7-2.0GeV
Q²:0.3-1.5GeV²
W:2.0-2.8GeV
Q²:0.3-1.5GeV²
NUMBER OF EVENTS/40MeV
10
0
40
20
0
40
20
0
04
08
12
16
20
Mπ⁺π⁻π°(GeV)

Fig.28

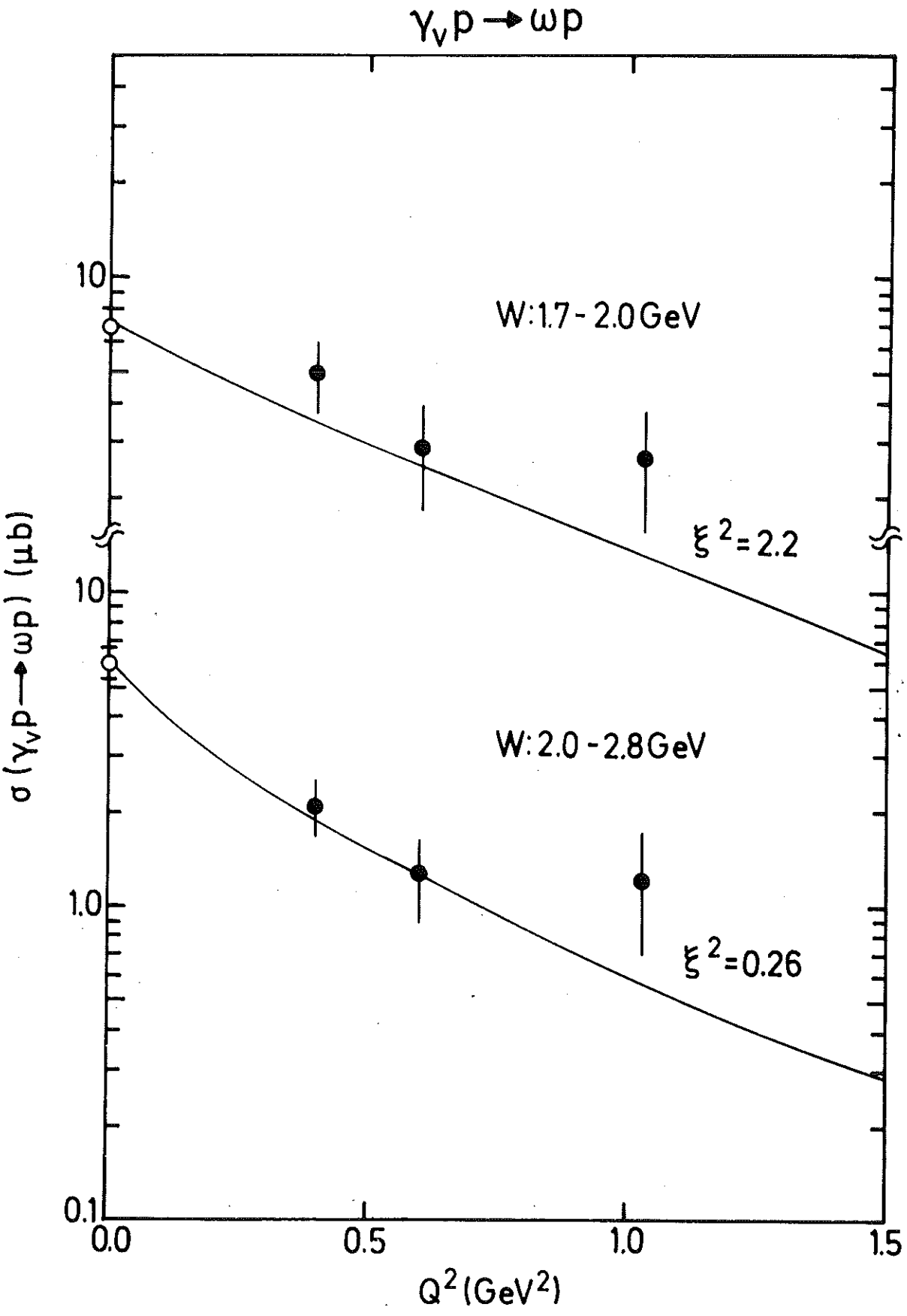
$\gamma_V p \rightarrow \omega p$
W:1.7 - 2.0GeV
$\xi^2 = 2.2$
W:2.0 - 2.8GeV
$\xi^2 = 0.26$
$\sigma(\gamma_V p \rightarrow \omega p)$ (μb)
Q^2 (GeV^2)
10
1.0
0.1
0.0
0.5
1.0
1.5

Fig.29

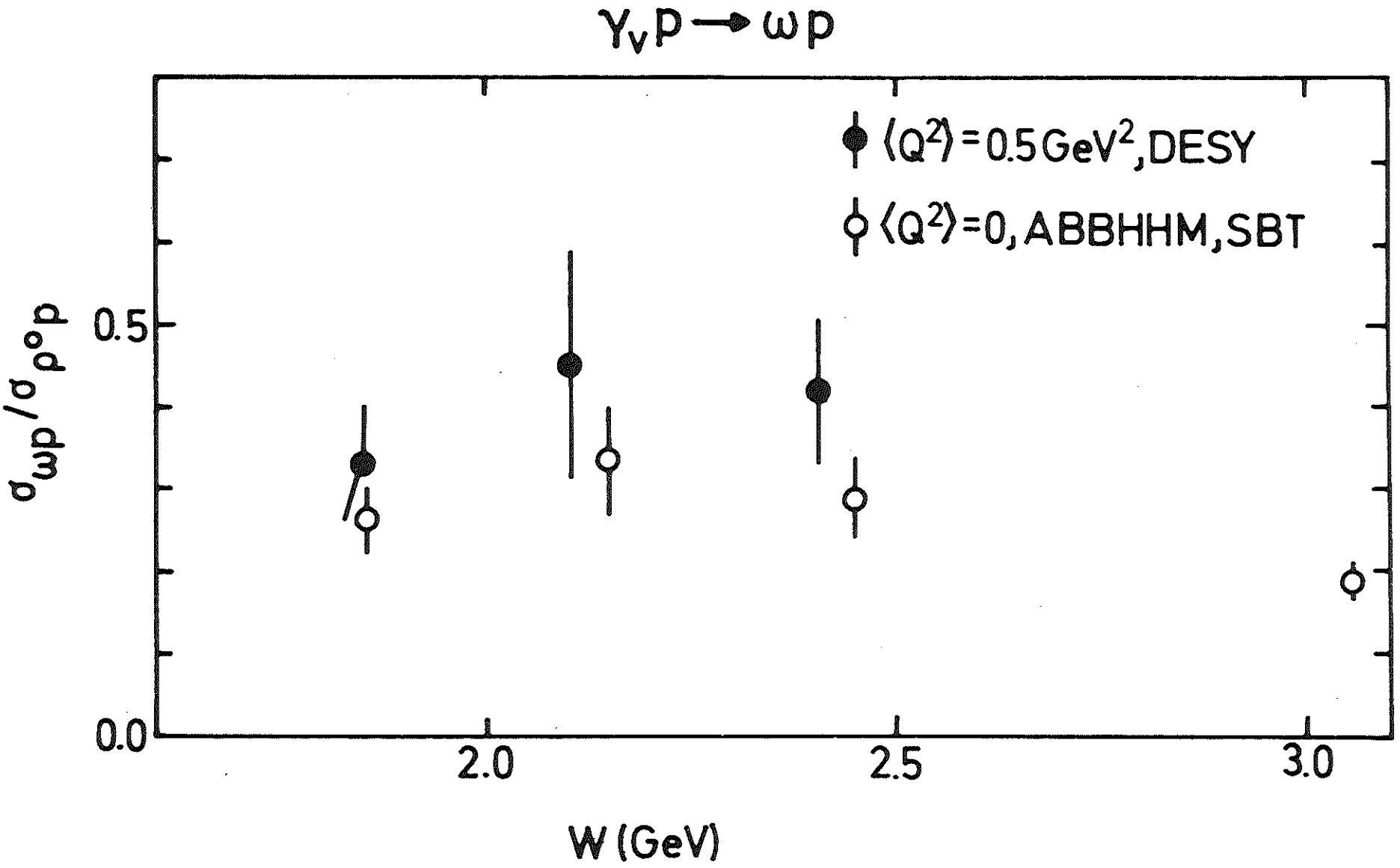
$\gamma_v p \rightarrow \omega p$
$\langle Q^2 \rangle = 0.5\,GeV^2$, DESY
$\langle Q^2 \rangle = 0$, ABBHHM, SBT
$\sigma_{\omega p} / \sigma_{\rho^0 p}$
0.5
0.0
2.0
2.5
3.0
W (GeV)

Fig.30